

Tectonics

RESEARCH ARTICLE

10.1029/2019TC005891

Key Points:

- Seismic interpretation and gravity inversion allowed to constrain the 3-D distribution of evaporitic detachments in the southern Pyrenees
- The South Pyrenean triangle zone terminates to the west at the transition from a ramp-dominated to a detachment-dominated triangle zone
- The overall structure is controlled by the presence and lateral variability of a multidetachment unit (Barbastro Fm.)

Supporting Information:

- Supporting Information S1
- Figure S1
- Figure S2
- Figure S2 (cont.)

Correspondence to:

P. Santolaria,
pablo.santolaria.otin@gmail.com

Citation:







Santolaria, P., Ayala, C., Pueyo, E. L., Rubio, F. M., Soto, R., Calvin, P., et al. (2020). Structural and geophysical characterization of the western termination of the South Pyrenean triangle zone. *Tectonics*, 39, e2019TC005891. <https://doi.org/10.1029/2019TC005891>

Received 23 SEP 2019

Accepted 15 JUN 2020

Accepted article online 22 JUN 2020

Structural and Geophysical Characterization of the Western Termination of the South Pyrenean Triangle Zone

P. Santolaria^{1,2} , C. Ayala³ , E. L. Pueyo^{1,4} , F. M. Rubio⁵, R. Soto^{1,4} , P. Calvin⁶ , A. Luzón⁷, A. Rodríguez-Pintó⁸, C. Oliván⁸, and A. M. Casas-Sainz⁷ 

¹Associated Unit in Earth Sciences IGME, University of Zaragoza, Zaragoza, Spain, ²Now at GEOMODELS Research Institute, University of Barcelona, Barcelona, Spain, ³Instituto Geológico y Minero de España (IGME), Madrid, Spain. Now at Geosciences Barcelona, CSIC, Barcelona, Spain, ⁴Instituto Geológico y Minero de España, IGME, Zaragoza, Spain, ⁵Instituto Geológico y Minero de España, IGME, Madrid, Spain, ⁶Departamento de Física, Laboratorio de Paleomagnetismo, Universidad de Burgos, Burgos, Spain, ⁷Departamento de Ciencias de la Tierra, Geotransfer Research Group, Instituto de Investigación en Ciencias Ambientales (IUCA), Universidad de Zaragoza, Zaragoza, Spain, ⁸Freelance geologist

Abstract The South Pyrenean triangle zone represents the southernmost front of the Pyrenees at its central portion deforming the Upper Eocene-Miocene Ebro Basin deposits. Two main structures characterize its western termination, the Barbastro anticline and the San Román backthrust, which detached on the Barbastro Formation (and lateral equivalents), an Upper Eocene-Lower Oligocene syntectonic evaporite-rich formation that acted as a multidetachment unit. Northward, the south directed Pyrenean thrust unit (i.e., Gavarnie-Sierras thrust sheet) detached along the Middle-Upper Triassic evaporitic rocks to finally ramp up and glide along the same Upper Eocene-Lower Oligocene multidetachment unit. A multidisciplinary approach allowed constructing a detailed structural and stratigraphic model of the study area. The workflow consisted of (1) constraining the geometry and structural architecture based on surface geology, interpretation of seismic lines (>900 km), and wells and (2) obtaining the 3-D density distribution of the multidetachment unit using gravity stochastic inversion (more than 7,000 gravity stations and 1,500 density data). The geometry of the sole thrust of the Gavarnie-Sierras thrust sheet was controlled by the distribution of the evaporite-rich units of the Barbastro Fm. Weak detachments promoted thrust salient formation and thrust flat geometries. The western termination of the South Pyrenean triangle zone is defined as a westward transition from a ramp-dominated and multiple triangle zone to a detachment-dominated one. Its geometry, kinematics, and location were controlled by the heterogeneous lithology of the Barbastro Fm. and its basal, halite-based detachment southern pinch-out.

1. Introduction

The occurrence of multiple detachments (i.e., a stratigraphic pile involving two or more décollement units) impacts the style of deformation in fold-and-thrust belts (e.g., Bonini, 2001; Cobbold et al., 2009; Cobbold & Rodrigues, 2007; Couzens-Schultz et al., 2003). This feature is relatively common in many fold-and-thrust belts worldwide: the Parry Island (Harrison, 1995), the Central Andes (Dunn et al., 1995; Pichot & Nalpas, 2009), the Rocky Mountains (e.g., Lebel et al., 1996), the Pyrenees (e.g., Muñoz, 1992), the Kuqa fold-and-thrust belt (e.g., Izquierdo-Llavall et al., 2018), the Zagros (Sherkati et al., 2006), the Apennines (e.g., Massoli et al., 2006), and the European Alps (Burkhard & Sommaruga, 1998; von Hagke et al., 2012). Most studies analyzing the effect of multiple décollements on the geometry and/or kinematics of fold-and-thrust belts deal with different detachment units at different stratigraphic levels (e.g., Bonini, 2001; Borderie et al., 2018; Couzens-Schultz et al., 2003; Massoli et al., 2006; Price, 1981; Santolaria et al., 2015). The mechanical stratigraphy of these systems, alternating ductile and brittle or weak and stiff units, favored tectonic wedging, delamination of the cover through weak detachments and the formation of triangle zones (von Hagke & Malz, 2018, and references therein). The term triangle zone has been used in the literature to define different structures. In this work we use the definition of triangle zone by von Hagke and Malz's (2018): "structures with a triangular shape in section view accommodating shortening by coeval

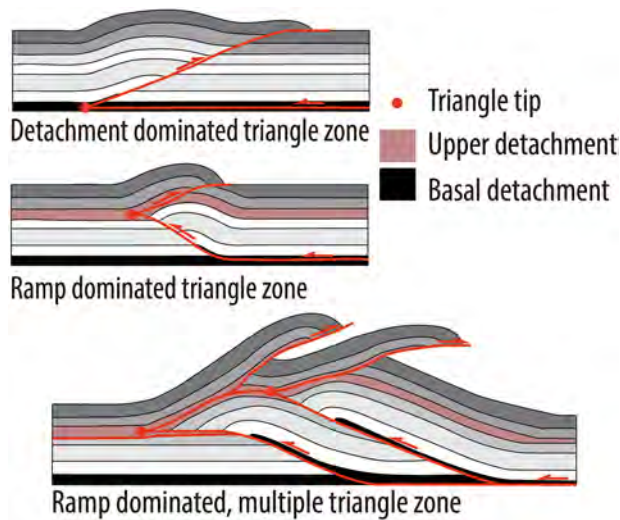


Figure 1. Sketch showing the geometry of detachment- and ramp-dominated triangle zones (after von Hagke & Malz, 2018) and a specific case illustrating a ramp-dominated, multiple-triangle zone. Simplified and modified from Couzens-Schultz et al. (2003), after Banks and Warburton (1986), Jones (1996), Bonini (2001), and von Hagke and Malz (2018).

activity of a basal thrust and an associated backthrust of opposite vergence.” These authors stress the importance to address, in addition to the geometrical analysis, the kinematic and mechanical implications when defining triangle zones. Depending on whether the triangle zone involves a single or two or more detachments, von Hagke and Malz (2018) classified triangle zones into detachment or ramp-dominated types, respectively (Figure 1).

The South Pyrenean triangle zone represents a good example to study the role played by syntectonic evaporitic units on folding and thrusting (Koyi & Sans, 2006; Krzywiec & Vergés, 2007; Sans et al., 1996; Vergés et al., 1992; Vergés & Burbank, 1996). The geometry, orientation and extent of the South Pyrenean triangle zone vary along strike, controlled by the thickness and distribution of the involved foreland syntectonic evaporitic units (Sans et al., 1996; Figure 2a). These units were deposited in the Ebro foreland basin, in marine and lacustrine areas laterally related to alluvial systems sourced in northern structures (Anadón et al., 1989; Muñoz et al., 2002; Pardo et al., 2004). Northward, the Pyrenean structures are characterized by their foreland vergence and detach along an older décollement unit, the Middle-Upper Triassic.

The eastern sector of the South Pyrenean triangle zone is wider than the western one, displays an array of structures and includes three, Lutetian to Lower Oligocene evaporitic units: Beúda, Cardona, and Barbastro Fms. (e.g., Ortí, 1988; Sans et al., 1996). To the west, the triangle zone narrows coinciding with the pinch-out of the older evaporitic unit. In the western sector of the South Pyrenean triangle zone, the younger evaporitic unit, the Barbastro Fm., acted as a multidetachment unit. This formation can be divided into several evaporitic subunits (Gil & Jurado, 1994; Sans et al., 1996) separated by interbedded terrigenous packages. The western sector of the South Pyrenean triangle zone is mainly characterized by a continuous structure whose geometry also changes along strike, the Barbastro anticline (Gil & Jurado, 1998; Martínez-Peña & Pocoví, 1988; Pardo & Villena, 1979; Riba et al., 1983; Sans, 2003; Senz & Zamorano, 1992).

This work, based on a multidisciplinary approach, is aimed to analyze the influence of evaporite-rich facies distribution on the structural style and kinematics of orogenic frontal structures, using the western termination of the South Pyrenean triangle zone as a study case. The implications obtained can be extrapolated to other triangle zones having multidetachment units. The subsurface geometry of the study area was reconstructed integrating surface geology and seismic reflection profiles supported by well data. Additionally, gravity data together with a large rock density data set were processed together to perform 3-D gravity stochastic inversion to map the 3-D distribution of the low-density packages within the Barbastro Fm. and laterally equivalent units. This new methodological approach allows understanding the 3-D distribution and the lateral density changes of the detachment levels and to evaluate its implications in the final architecture. Finally, we discuss the kinematic and mechanical implications of the new definition of the Barbastro anticline structure.

2. Geological Setting

2.1. Geological Setting of the Study Area

The study area encompasses the western termination of the South Pyrenean triangle zone (Figure 2a). It is located in the South Central Pyrenees between the southernmost Pyrenean thrust sheets and the autochthonous deposits of the Ebro foreland basin.

The WNW-ESE trending Pyrenean range grew as an asymmetric doubly verging wedge (e.g., Choukroune & ECORS team, 1989; Martínez-Peña & Casas-Sainz, 2003; Muñoz, 1992; Roure et al., 1989; Teixell, 1998; Vergés & García-Senz, 2001) as a result of the convergence and collision between the Iberian and European plates from Late Cretaceous to Early Miocene times (e.g., Muñoz, 2002; Roest & Srivastava,

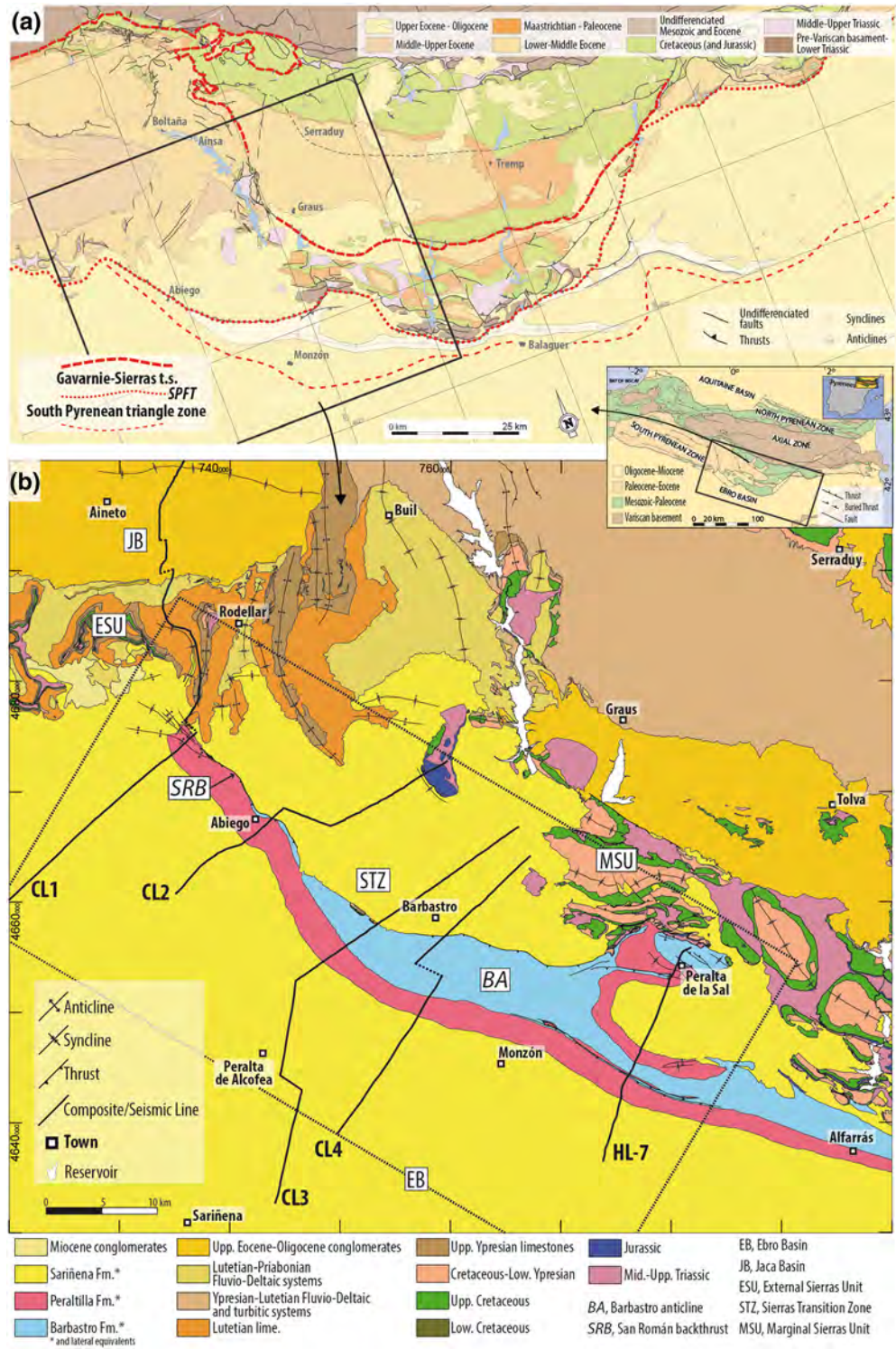


Figure 2. (a) Geological map of the South Central and Eastern Pyrenees. The limits of the Gavarnie-Sierras thrust sheet and the South Pyrenean triangle zone are shown by dashed red lines (modified from Muñoz et al., 2018; after Sans et al., 1996). (b) Simplified geological map of the studied area, see gray frame in (a) and Pyrenean regional map (center-right) for location.

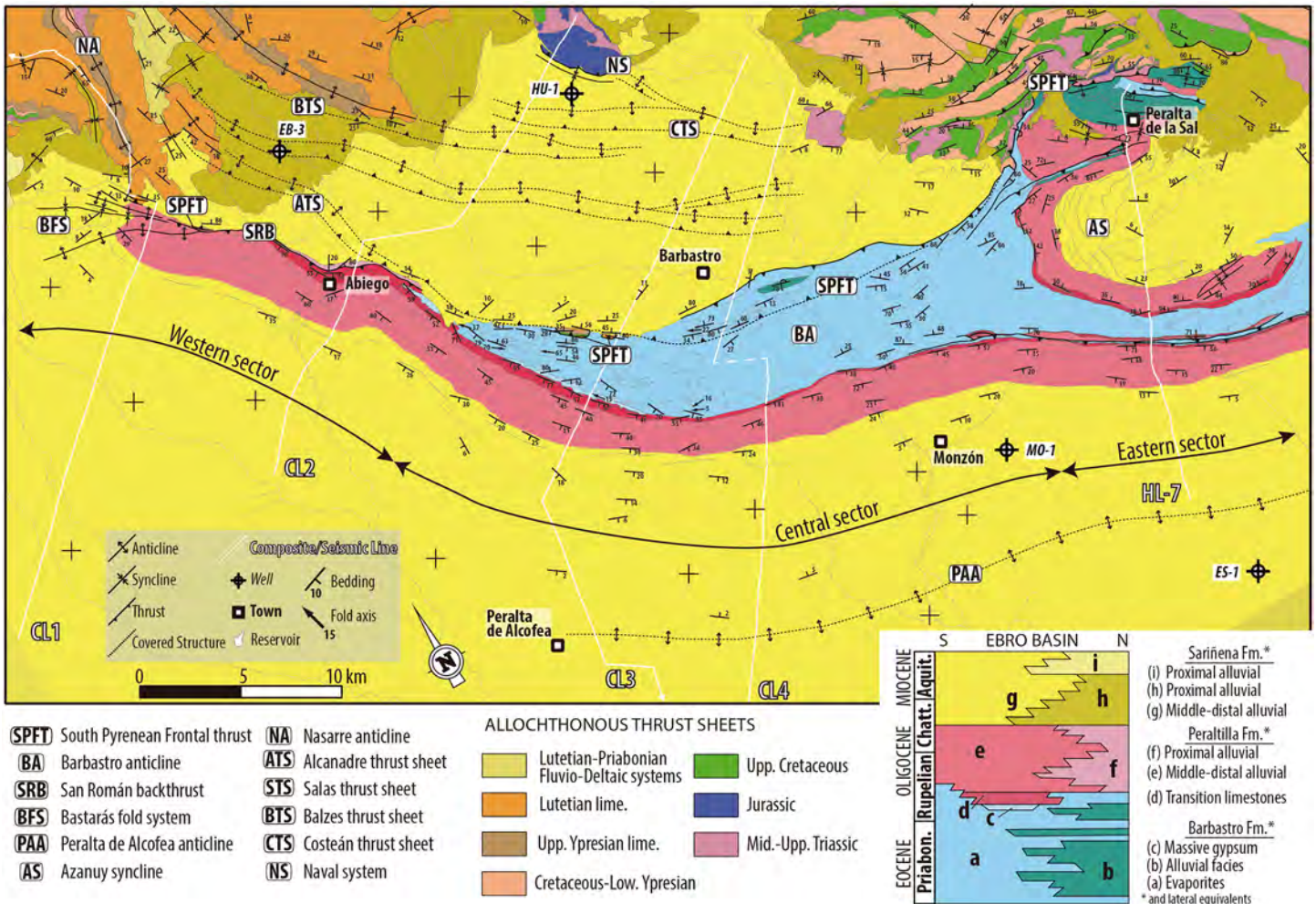


Figure 3. Detailed geological map of the western termination of the Barbastro anticline. Numbers indicate the main structural features referred to in the text. Thin black lines denote outcropping structures, while dashed black lines refer to covered structures.

1991; Rosenbaum et al., 2002). The South Central Pyrenees salient is constituted by three main thrust sheets, detached from the basement along the Middle-Upper Triassic décollement (Muñoz et al., 2013). The Gavarnie-Sierras thrust sheet is the southernmost (Figure 2a, red dashed lines) and youngest one (Lutetian to Oligocene, see Millán-Garrido et al., 2000; Muñoz et al., 2013; Oliva-Urcia, 2018). It comprises, along strike, the following structural units: Marginal Sierras in the east, the External Sierras in the west, and their connection, herein named the Sierras Transition Zone (STZ) (Figure 2b).

The Marginal Sierras unit (Pocoví, 1978, 1979) is a thrust system which records out-of-sequence thrusting and thrust reactivations. It displays a decreasing spacing trend between tectonic structures (from 5 to less than 1 km) toward the south. Widespread outcrops of Middle-Upper Triassic rocks reveal a thickened décollement underneath this unit (Santolaria et al., 2016). The tectonic structures plunge toward the WNW in the western edge of the Marginal Sierras unit and are covered by Oligocene-Miocene rocks in the STZ (Figure 2b). In this latter unit, the allochthonous stratigraphic units crop out at the borders of Triassic salt diapirs and at the South Pyrenean Frontal Thrust (SPFT) (Figure 3), the surficial expression of the South Pyrenean Sole Thrust (SPST). To the north of the STZ and in the External Sierras a series of evenly spaced, N-S trending, detachment and fault-propagation folds stand out; they underwent vertical axis rotations during the Eocene-Oligocene (Mochales et al., 2012, 2016; Muñoz et al., 2013; Pueyo et al., 2002; Rodríguez-Pintó et al., 2016). One of these folds, the Balzes anticline (Rodríguez-Pintó et al., 2016)

changes its trend from N015E in its northern part to N142E in its southern part, where it parallelizes the Barbastro anticline (Figure 3).

The SPFT displays several salients and reentrants and is partly covered by the Oligo-Miocene syntectonic alluvial deposits belonging to the Ebro Basin foreland succession. Right to the south, the Barbastro anticline (Selzer, 1934) and the San Román backthrust (Martínez-Peña, 1991; Millán, 1996; Navarro, 1987; Puigdefàbregas, 1975) represent the southernmost Pyrenean tectonic structures in this sector (Figure 3).

2.2. Stratigraphy

In the Gavarnie-Sierras thrust sheet, the stratigraphic succession (Figures 3 and 4) includes Middle-Upper Triassic evaporites and mudstones, rare Jurassic limestones, Santonian to Maastrichtian limestones, conglomerates and sandy limestones, Maastrichtian to Paleocene red beds and fresh water limestones (Garumnian Facies), and lower Ypresian limestones (Garrido-Megías & Ríos-Aragües, 1972; Muñoz et al., 2013; among others). The uppermost Ypresian to Lutetian limestones built up the mountainous reliefs of the External Sierras; they integrate a decameter-thick unit cropping out in the STZ frontal structures and are not represented in the Marginal Sierras. Upper Lutetian to Priabonian transitional sandstones grading into mainly mudstones and sandstones (Hogan & Burbank, 1996) top the succession. Finally, Oligocene-Miocene detrital facies filling the foreland basin unconformably cover the previously described units, the STZ and the SPFT (Figure 3).

In the foreland basin, Upper Priabonian-Middle Rupelian tabular, generally decimeter-thick, gypsum levels with interbedded gray, and subordinate red, mudstones (Lucha et al., 2012; Luzón, 2001) integrate the Barbastro Fm. (Quirantes, 1969), which represents lacustrine evaporite deposition; locally, massive gypsum packages are present (Barnolas, García-Sansegundo, et al., 1990). In the southeastern part of the studied area, the evaporite formation grades northward (close to the Marginal Sierras unit) into alluvial facies (mainly mudstone and locally derived breccias), but in the lower part of this alluvial succession, 90 m of massive salts has been identified in wells (Senz & Zamorano, 1992). The Barbastro Fm. is covered by Oligocene-Miocene, north-derived detrital deposits (conglomerate, sandstones, mudstones) belonging to the Peraltilla (Middle Rupelian to Chattian, Crusafont et al., 1966) and Sariñena (Chattian to Aquitanian, Quirantes, 1969; Cuenca et al., 1992) Fms. This transition reflects a progradation of the pyrenean alluvial systems and the disappearance of the evaporite lake. Decimeter-thick lacustrine limestone and gypsum levels are locally interbedded in the detrital succession (see Senz & Zamorano, 1992 and Luzón, 2005 for further details). It is worth noting that a 30–120 m thick (Barnolas, García Senz, et al., 1990) package of lacustrine limestones and mudstones with sandstones and rare gypsum represents the transition from the Barbastro Fm. to the Peraltilla Fm.

In the subsurface, the Monzón-1 [MO-1] (Figure 3) well reveals an 886 m thick unit corresponding to the Barbastro Fm. (Figure 4a). It is integrated by gypsum and marls with interbedded decameter-thick halite and anhydrite packages; a 90 m-thick massive gypsum level tops the unit. Toward the NW, in the Huesca-1 [HU-1] well (Figures 4a and 4d), detrital facies laterally equivalent to the Barbastro Fm. lie on a 100 m thick level of halite and gypsum labeled as the Ebro Basin basal detachment in Figure 4a. The subsurface stratigraphy of the Ebro foreland basin in the study area is known from three exploration wells (Gil & Jurado, 1998; Lanaja, 1987) (Figures 4a and 4d for location) that reveal that the Barbastro, Peraltilla and Sariñena Fms. unconformably overlie the Triassic to Lower Eocene sequence (Figure 4a).

2.3. The Barbastro Anticline and the San Román Backthrust

The Barbastro anticline is a WNW-ESE trending, 90 km long structure that runs approximately parallel to the SPFT, mimicking the curvature of the South Central Pyrenean salient (Figure 2a). To the east, where the South Pyrenean triangle zone widens, it branches into several thrusts and folds (Sans et al., 1996) (Figure 2a). In the study area, the Barbastro anticline narrows progressively to the west, changes its trend from a N120°E to a N150°E and joins finally with the San Román backthrust (Martínez-Peña & Pocoví, 1988, Figures 2b and 3).

The anticline is cored by the Barbastro Fm. (Martínez-Peña & Pocoví, 1988). In its southern limb, the Peraltilla Fm. strata are arranged in a 30° to 60° (eventually subvertical where in contact with the Barbastro Fm.) south dipping panel (Barnolas, García-Sansegundo, & Teixell, 1990) (Figure 3). Still farther

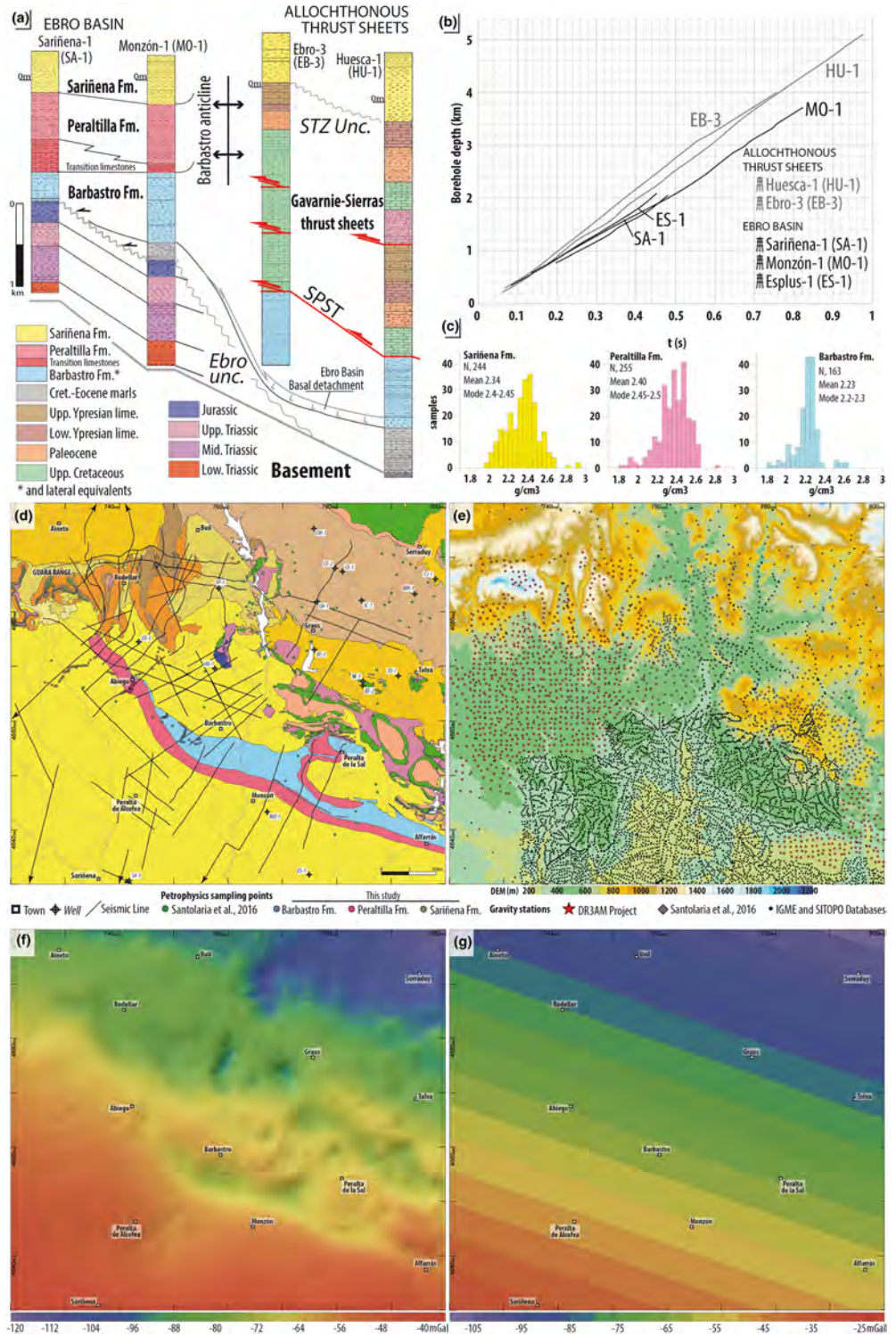


Figure 4. (a) Correlation of lithological logs of the key available wells in the area. (b) Depth to time graphs synthesized from sonic log data coming from wells located near the Barbastro anticline. (c) Frequency diagrams of density measurements of the Ebro Basin units; for further information see Pueyo et al. (2016) and Santolaria et al. (2016). (d) Location of interpreted seismic lines, petrophysical sampling points and wells; geological map at the background. (e) Gravity stations classified by surveys; contoured digital elevation model at the background. (f) Bouguer and (g) regional gravity anomaly maps.

south, beds of the Sariñena Fm. conformably cover the Peraltilla Fm. deposits and become progressively horizontal.

The western termination of the Barbastro anticline links with the San Román backthrust, that passes eastward to the Bastarás fold system (Figure 3, western sector, McElroy, 1990). To the west of the central sector, the core of the anticline is characterized by (i) vertical or south verging, tight to isoclinal, meter to decameter-scaled folds in the gypsum-dominated packages and (ii) tight to gentle folds (and seldom thrusts) with no dominant vergence in mudstone-dominated levels (Barnolas, García-Sansegundo, & Teixell, 1990; Pardo & Villena, 1979). To the east of the central sector, the northern flank of the Barbastro anticline presents a south dipping overturned panel, which involves well-bedded gypsum and interbedded sandstones (Figure 3, central sector). In the eastern sector, from north to south, the Ebro Basin units are deformed by a sequence of SW verging thrusts, a tight, NE verging anticline which is truncated to the south by a W-E trending backthrust that becomes blind to the east, and finally the Azanuy syncline, an 8 km wide gentle syncline, in whose northern flank the Sariñena Fm. laps onto the Peraltilla Fm. (Senz & Zamorano, 1992, Figure 3). In this sector, in the southern flank of the Barbastro anticline, a 15 km long, 500 m wide outcrop of the lower part of the Peraltilla Fm. has been interpreted as belonging to a downward facing hanging-wall (Sans et al., 1996); evaporites display here meter- to decameter-scale, south verging east plunging folds (Pardo & Villena, 1979; Sans et al., 1996).

3. Data and Methods

This work integrates surface and subsurface data coming from different surveys and methods (Figure 4). Surface data (stratigraphic and structural measurements) consist of 2,810 bedding measurements (Barnolas, García-Sansegundo, & Teixell, 1990; Barnolas, García Senz, et al., 1990; Barnolas, Teixell, et al., 1990, 1994; GEODE, 2011; Martínez-Peña & Pocoví, 1988; McElroy, 1990; Millán, 1996; Luzón, 2005; Rodríguez-Pintó, 2012; Santolaria et al., 2016; Senz & Zamorano, 1992; this work) compiled in a geological map (Figures 2b and 3). Subsurface information comes from five exploration wells (Figures 4a, 4b, and 4d) for location), seismic reflection profiles (Figure 4d), and gravity data (Figure 4e). Petrophysical information (Figures 4c and 4d for sampling locations) includes density data coming from Santolaria et al. (2016), Pueyo et al. (2016), and new measurements carried out in this work. The workflow consisted of (1) constraining the structure from surface geology, seismic reflection profiles, and well data complemented with gravity maps and (2) obtaining the 3-D density distribution of the Barbastro Fm. and lateral equivalents using gravity inversion. The density contrast between evaporitic units (Triassic and Eocene, $[c]2.25 \text{ g/cm}^3$) on one side and nonevaporitic rocks (e.g., Oligocene detrital facies, $[c]2.40 \text{ g/cm}^3$; Cretaceous limestones, $[c]2.67 \text{ g/cm}^3$) or basement rocks ($[c]2.75 \text{ g/cm}^3$) on the other, makes possible to use the gravimetric method (Calvín et al., 2018; Izquierdo-Llavall et al., 2019; Pinto et al., 2005; Santolaria et al., 2016). In this work, the gravimetric data set has a dense coverage (more than 1 point per km^2) that allowed to model evaporite units and to detect lateral facies changes. This approach represents an efficient tool to assess the 3-D distribution of evaporite-rich detachments and allows to discuss its impact in the structural style and evolution of fold-and-thrust belts.

3.1. Seismic Reflection Profiles and Well Data

A total of 42 two-dimensional seismic reflection profiles (totaling more than 900 km, Figure 4d) was compiled from a public database repository (info.igme.es/SIGEOF/) and interpreted in this study. The most representative lines are here shown as composite lines (CL1 to CL4) or as a single line (HL-7). The density of seismic profiles is high, with low-medium quality and heterogeneous seismic processing. This drawback was solved thanks to feedback between seismic interpretation and gravity modeling. Available seismic sections are high-resolution tiff files showing shot points location. They were vectorized and converted into segy files by means of Image 2seg software developed by the Institut de Ciències del Mar (CSIC; Farran, 2008) and then reduced to a common datum by means of the Kingdom Suite software (by IHS Markit) where they were interpreted.

Interpretation of seismic reflection profiles was constrained with five exploration wells (Figure 4a for lithological logs; Figure 4d for location). Apart from the lithological description of the logs, synthesized by Lanaja (1987) and partially reinterpreted in this work, partial density and sonic logs are also available (info.igme.es/SIGEOF/).

3.2. Time-to-Depth Conversion and 3-D Reconstruction of the Study Area

We performed the time-to-depth conversion to avoid structural ambiguities and to provide a depth basis for gravity inversion and cross-section restoration. Time-to-depth conversion was based on a 3-D velocity model represented by a velocity voxel built from (i) sonic logs (Figure 4b)) and (ii) key structural and stratigraphic time-based surfaces (see supporting information for further details). The depth-time curves corresponding to the Ebro Basin wells exhibit gentler slopes than lines of the STZ wells (Figure 4b). Applying a linear regression, we obtained a simplified seismic velocity of 4,387 and 5,226 m/s, respectively for the two areas. This points out the necessity of considering two different seismic velocity domains, and consequently we ruled out a simplistic time-to-depth conversion approach (Figure S1, supporting information).

Interpreted horizons (as XY-Time point clouds) were converted through the seismic velocity voxel (Figure S1, supporting information) and the output depth-based horizons double-checked against the actual well depth. Misfits between depth converted horizons and true depth are below 80 m in the Gavarnie-Sierras Unit and below 130 m in the Ebro Basin continental sequence. Finally, depth-based point clouds were used to construct key structural and stratigraphic surfaces.

3.3. Gravity Data, 3-D Gravity Inversion, and Density Data

A total of 7,376 gravity stations was used to obtain the Bouguer anomaly (Figure 4f): 5,469 stations from IGME and SITOPO databases (Ayala et al., 2016), 903 stations from Santolaria et al. (2016) and 1,004 new stations acquired in this work. Up to six anchor points together with areal overlapping between different surveys were considered to ensure a robust link between datasets. In addition, the new data were processed using the same parameters as the ones used for the gravity stations from the databases. We did not detect any mismatch between the different surveys and consequently the three data sets were merged to obtain a continuous, harmonized Bouguer anomaly map. To model relatively shallow density variations, a residual gravity anomaly was obtained by subtracting from the Bouguer anomaly a linear regional field (displaying a N120°E trend) that reflects the contribution of the structures in the middle to lower crust and upper mantle.

Previous 2.5-D gravity forward modeling in the study area (Santolaria et al., 2016) highlighted the necessity of considering a density variation (from 2.2 to 2.5 gr/cm³) within the Upper Eocene units (basically Barbastro Fm. and lateral equivalents). For this reason, we performed a complete 3-D gravity inversion specifically focused on these geological units. The 3-D gravity model was obtained by stochastic inversion using 3-D GeoModeller software from Intrepid Geophysics (e.g., Guillen et al., 2008). The model is based on key stratigraphic and structural surfaces coming from the interpolation of the interpreted and depth-converted seismic horizons.

The 3-D gravity model has dimensions of 80 × 70 km (5,600 km²), its top is at the topographic surface (that comes from a 100 m accuracy digital elevation model, Figure 4e) and the bottom is at −6,500 m, including the upper part of the Paleozoic basement. To carry out the inversion, each unit is discretized in voxels of 500 × 500 × 200 m. The total number of cells is 1,008,000 (160 × 140 × 45 cells); in each cell the density value was assigned according to its unit.

The 3-D gravity model includes 290 representative bedding dips, contacts of target units, and the main faults and thrusts traces. Density data come from a petrophysical dataset (>3,000 density values): 1,109 samples from Santolaria et al. (2016), 429 additional samples acquired during this study (Figure 4c), and density data from the Iberian Range and Ebro Basin (Pueyo et al., 2016). The stratigraphic pile was divided into seven units, each characterized by its density range: (1) Basement, (2) Triassic-Jurassic rocks of the Ebro Basin, (3) autochthonous Cretaceous to Eocene, (4) Barbastro Fm. and lateral equivalents, (5) Oligocene-Miocene terrigenous units (Peraltilla and Sariñena Fms.), (6) Middle-Upper Triassic evaporites, and (7) nonevaporitic rocks involved in the Gavarnie-Sierras thrust sheets.

In the GeoModeller software, the calculations of the inversion are based on the Monte Carlo Markov chain method (Tarantola, 2005), a well-known and widely used mathematical method in geophysical inversion (e.g., Anderssen et al., 1972; Anderssen & Seneta, 1971; Keilis-Borok & Yanovskaya, 1967; Press, 1968, 1970). It consists of minimizing the gravimetric misfits (difference between observed and calculated gravity anomalies) by changing the lithological boundaries, the density or both parameters in each iteration. In this case, we considered the geometry to be well constrained by the seismic profiles and allowed varying only the

density. The main objective was to delineate the distribution of low-density materials within the Barbastro Fm. and lateral equivalents which tentatively would correspond to evaporite and terrigenous facies, respectively. This method allowed constraining the density variations within the target unit as a whole and, therefore, specific evaporitic detachments (subunits within the target) cannot be discretized. In other words, as set, this method allows to detect lateral density variations rather than vertical changes. Thus, we have allowed densities to vary within $\pm 0.01\text{--}0.08\text{ g/cm}^3$ except for the Barbastro Fm. and lateral equivalents where densities can vary within $\pm 0.15\text{ g/cm}^3$. The inversion was run for 25×10^6 iterations and at the end of the inversion, the RMS of the misfits (difference between observed and calculated residual anomaly) was 0.43 mGal. A thorough description of the modeling process can be found in Guillen et al. (2008).

4. Bouguer and Residual Gravity Anomaly Map

The Bouguer anomaly map shows a long wavelength gradient displaying a decreasing trend from NW to SE and ranging from -120 to -40 mGal (Figure 4f). Superimposed on this gradient (regional signature, Figure 4g), there are relative maxima and minima of medium to short wavelength associated with local density variations mainly related to (1) Triassic salt accumulations within the Pyrenean thrust sheets and (2) Eocene evaporites in the Barbastro anticline (see Santolaria et al., 2016 for further details). The residual anomaly map (Figures 5a and 5b) shows gravity values ranging from -17 to 12 mGal. In the northern part of the studied area, values change from positive to negative from west to east (Figure 5a, A and B labels, respectively). The central area features several N110°E to N130°E trending, short to medium wavelength highs and lows. To the east, a continuous gravity high (10 mGal) stands out among surrounding gravity lows (Figure 5a, C label). Westward, a series of constantly spaced (≈ 11 km) gravity lows are aligned N100°E (Figure 5a, D label). Among them, the lowest values (-17 mGal) correlate with Triassic salt diapirs and with the southernmost portions of the Balzes (-10 mGal) and Nasarre (-4 mGal) anticlines, thus suggesting the presence of Triassic low-density rocks in their cores. To the south, the residual anomaly is characterized by a trendless distribution of highs and lows (Figure 5a, E and F labels). In the Marginal Sierras, gravity lows broadly coincide with Triassic evaporites accumulations (Figure 5a, E label), whereas in the STZ positive values dominate (Figure 5a, F label) suggesting smaller volumes of low-density rocks underneath.

To the south, a N100°E elongated, continuous gravity low (-14 mGal) almost perfectly matches the outcrop of the Barbastro Fm. (Figure 5a, label G and Figure 5b). The southern boundary of this gravity low mimics the limit between the Barbastro and Peraltilla Fms. Its northern limit features two positive salients: (i) the eastern one correlates with the Azanuy syncline and (ii) the western one has no direct correlation with the evaporites of the Barbastro Fm. The second observation implies the necessity to consider a relative high-density body below the outcropping Barbastro Fm. evaporites. Note how the anomaly associated with the Barbastro anticline is reduced to a relatively narrow low toward the edge of the study area where the expected low gravity signal is overprinted by the closeness of the Marginal Sierras Unit. To the west of sector G, the gravity low gradually disappears as the Barbastro anticline laterally passes to the San Román back-thrust and its gravity signal becomes part of a widespread (3 to 9 mGal) plateau in the Ebro Basin (Figure 5a, label H). Southeast of this plateau, gravity values abruptly drop to define a 17 km wide, N045° E trending gravity low (-8 mGal, Figure 5b, I label). In turn, to the east, this gravity low progressively passes to a relative high (Figure 5a, J label). This trimodal pattern within the Ebro Basin may respond to subsurface-related density variation since at surface, only flat-lying, homogeneous Oligocene to Quaternary alluvial-fluvial sediments crop out (Figure 5b).

5. Geometry From Seismic Profiles

5.1. Seismic Stratigraphy

The interpretation of available seismic profiles, wells and surface data allowed distinguishing the following seismic sequences, characterized by different reflectivity patterns and seismic facies (Figure 6): (1) the Paleozoic basement, (2) the Lower Triassic to Jurassic succession, (3) the Cretaceous to Eocene marine limestones and marls, (4) the Barbastro Fm. evaporites and their laterally equivalent terrigenous facies, and (5) the Oligocene-Miocene alluvial deposits belonging to the Peraltilla and Sarriena Fms. The Paleozoic basement (1) is represented by transparent seismic facies. Upward, a medium to high reflectivity package showing disrupted reflectors represents unit (2). Unit (3) is imaged as a high-reflective package displaying parallel

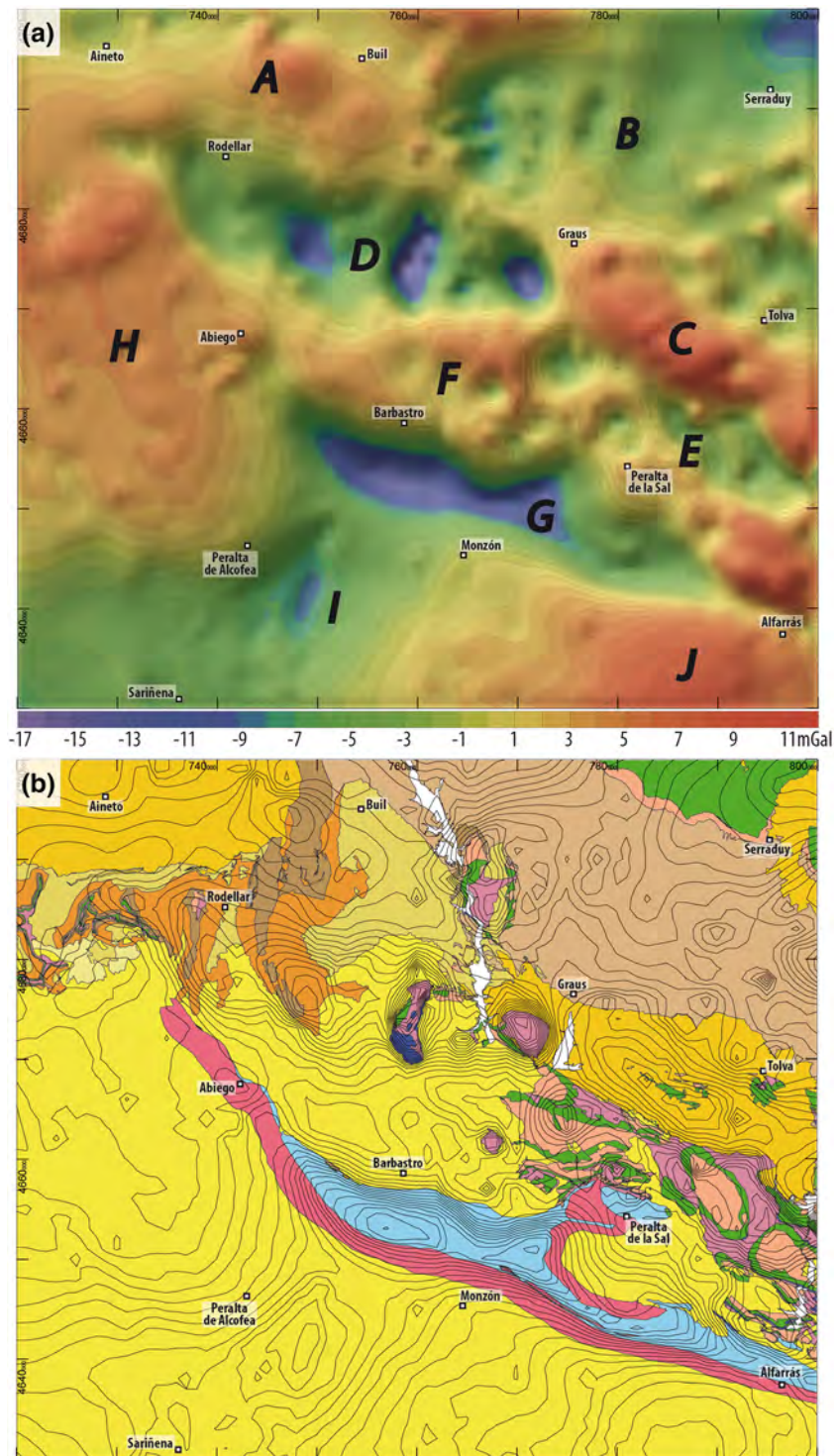


Figure 5. (a) Residual gravity map. To facilitate the correlation with surface geology, residual anomaly contours are plotted together with the geological map (b). Capital letters in (a) label the features referred to in the text.

and continuous reflectors that thicken toward the north. The Barbastro Fm. evaporites and their lateral stratigraphic equivalents (4) display parallel reflectors with different reflectivity, from base to top, they are: BFm1, a poorly reflective to transparent package; BFm2, a relatively thin group of continuous reflectors that may change laterally into semitransparent seismic facies; BFm3, a transparent package

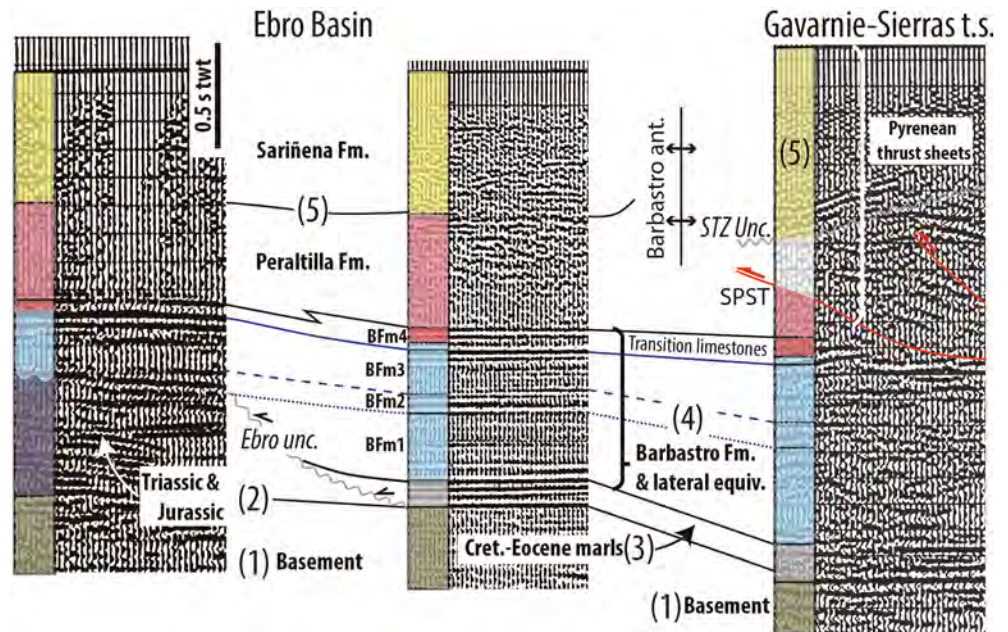


Figure 6. Main seismic packages and facies (labeled 1 to 5) and key horizons by structural domain: Ebro Basin (left and center) and Gavarnie-Sierras thrust sheet (right).

with scarce, discontinuous reflectors topped by a thin, highly reflective set of two reflectors, and BFm4, with variable thickness and showing a series of well-developed, parallel, and continuous reflectors, displaying in places semitransparent facies at its base. In the Ebro Basin, these subunits are relatively easy to recognize but, conversely, in the Barbaastro anticline and underneath the Gavarnie-Sierras thrust sheet, these reflectors are scarcer and display poorer definition (Figure 6). Transparent to semitransparent subunits (BFm1 and almost all BFm3) are interpreted as evaporite-rich intervals whereas subunit BFm2 and the top of BFm3 may correlate with denser lithologies. Finally, BFm4 coincides with the uppermost Barbaastro Fm. where the reflective succession corresponds to limestones, sandstones and mudstones and the underlying semitransparent facies is likely linked to massive gypsum (Figure 3; see also seismic detail in CL2, Figure 7). To simplify the stratigraphic interpretation, BFm4 also includes the transition to the overlying Peraltilla Fm. represented in most of the area by alternating limestones and mudstones. It is worth mentioning that the seismic facies-lithology correlation should be taken with caution since lateral lithology facies transition may occur (see below). The topmost unit (5) is a poorly reflective package with scarce, discontinuous reflectors. This unit correlates with conglomerates, sandstones and mudstones of the Peraltilla and Sariñena Fms. whose limits can be tracked from surface geology in the Ebro Basin but not in the Gavarnie-Sierras thrust sheet where they are labeled generically as Oligocene-Miocene (Figure 7). Time-based thicknesses of these Ebro Basin units and subunits change laterally. BFm1 ranges from 480 ms in the west to 130 ms to the east and disappears to the south. BFm2 presents a trendless thickness variation between 88 to 120 ms whereas BFm3 and BFm4 thicken to the east from 170 to 220 ms and 91 to 140 ms, respectively. The topmost unit (5) reaches a maximum thickness of 1,270 ms. Note that these time-based thicknesses are a function of the true stratigraphic thickness and the seismic velocity.

In the Ebro Basin, the five seismic packages are well represented (Figure 6). The Barbaastro anticline is generally characterized by chaotic to transparent seismic facies. However, some scarce and discontinuous reflectors can still be drawn in the Barbaastro anticline and correspond to reflective subunits within the Barbaastro Fm., as BFm2 and/or BFm4. In the Gavarnie-Sierras thrust sheet, a set of parallel reflective horizons appears commonly disrupted by faults or stratigraphic truncations. They are located on top of parallel reflectors representing the autochthonous deposits of the Ebro Basin. In the Pyrenean domain, seismic imaging is poor and further interpretations must be derived from surface geology and wells. The Middle-Upper Triassic

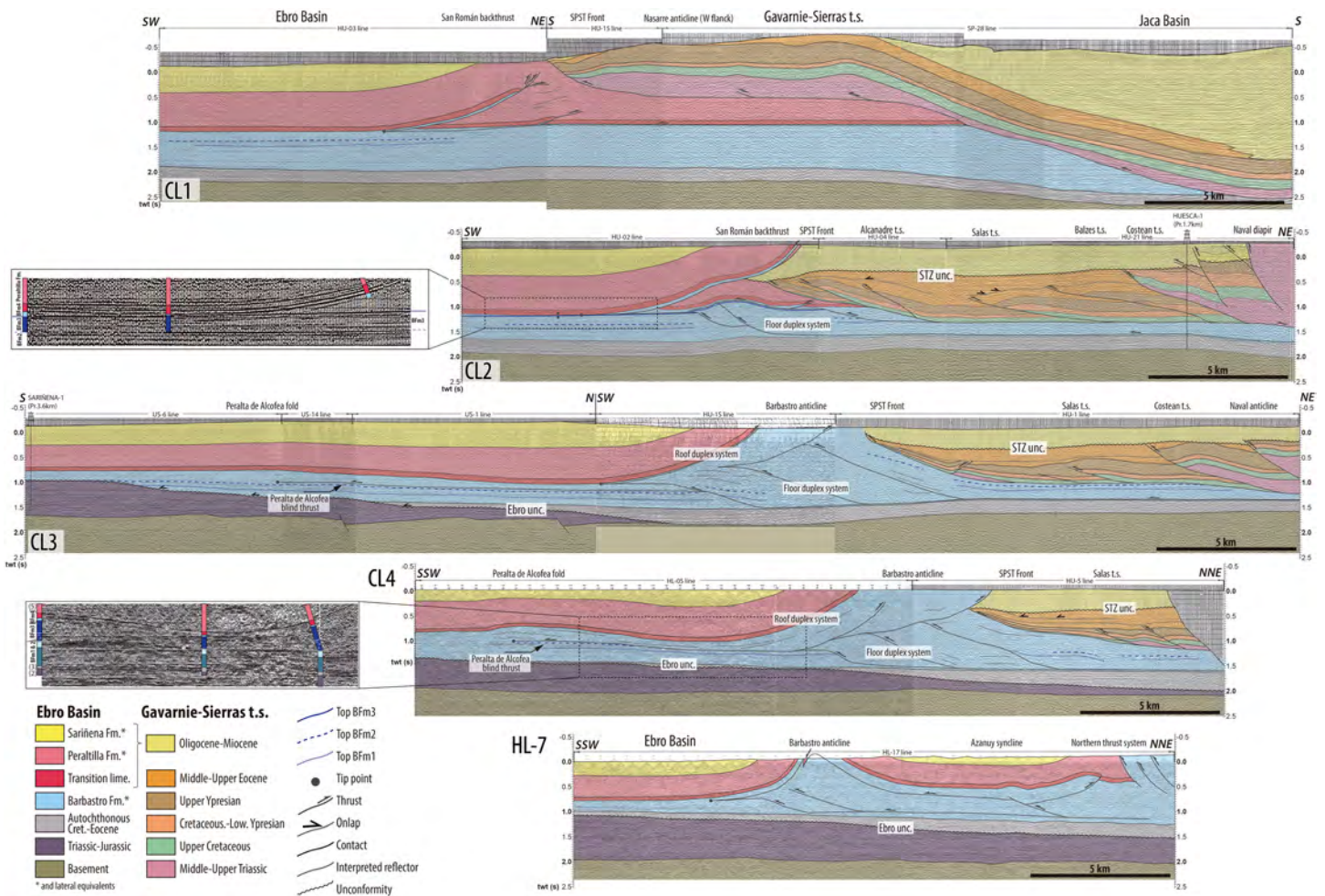


Figure 7. CL1, CL, CL3, and CL4 composite lines (this work) and HL-7 seismic profile (interpretation after Sans et al., 1996) illustrating the lateral variation of the Barbastro anticline and the San Román backthrust. Vertical scale in two-way time. See Figure 2b for location. Zoomed-in details highlight thinning-thickening trends within the Barbastro Fm. Original seismic composite sections are found in Figure S2; see supporting information.

evaporites are recognized as chaotic seismic facies occurring in some specific structures such as salt diapirs or within the core of hangingwall anticlines.

5.2. Seismic Profile Interpretation

5.2.1. Seismic Composite Line-1; External Sierras and Western Termination of the San Román Backthrust

To the north, flat-lying, well-defined reflectors become a north dipping panel that parallelizes (dorsal block) the SPST underneath and defines the southern limb of the Jaca Basin synclinorium (Figure 7, CL1). To the south, the SPST flattens. The structure of the External Sierras is poorly imaged and shows the flat-lying reflectors of the western flank of the Nasarre anticline. Below the Cretaceous to Lutetian sequence, Triassic evaporites represent about one third of the cover, which explain the -3 mGal gravity low. To the south, the SPFT truncates the Peraltilla and Sariñena Fms., whose reflectors define a south dipping panel interpreted as the template of the hanging wall ramp of the San Román backthrust where the Bfm4 is involved (Figure 7, CL1, HU-03 seismic line). The backthrust splays into secondary thrusts which pass to a fold system at surface. Underneath the San Román backthrust, highly reflective seismic facies having flat-lying reflectors depict no evidences of deformation (except for a small scale thrust) and continue the north, below the SPST, where their definition is poorer. The San Román backthrust roots in the southern tip point of a north directed, flat-lying thrust that links, through Bfm4, with the SPST (e.g., McElroy, 1990; Millán, 1996). To the south, reflectors in the Ebro Basin are mainly horizontal.

5.2.2. Seismic Composite Line-2; San Román Backthrust and Sierras Transition Zone West

To the north, Triassic evaporites in the Naval diapir feature chaotic seismic facies bounded by a nearly vertical thrust that truncates the Sariñena Fm. (Figure 7, CL2). South of the diapir, the structure is constrained by the HU-1 well. The Triassic to Early Ypresian sequence is duplicated by the Costeán thrust (this study). The hanging wall sequence is fossilized by the STZ unconformity, which is truncated by a secondary thrust. The SPST is drilled at $-3,068$ m (time equivalent: 1.4 s) and the basement is recognized at $-4,458$ m (time equivalent: 1.8 s). In contrast to CL1, the SPST here detaches along BFm1 rather than along BFm4. The SPST shows a flat geometry to finally ramp over the Barbastro and Peraltilla Fms., right to the North of an incipient Barbastro anticline where it is fossilized by the STZ unconformity. Rooted in the SPST, several north dipping thrusts (Balzes, Salas, Alcanadre sheets) involve a southward-thinning Cretaceous to Eocene succession. These thrusts die out into Middle-Upper Eocene units, which show wide, gentle folds locally truncated or covered by younger Eocene units. Nearly horizontal reflectors corresponding to Oligocene-Miocene rocks lie unconformably at their top.

The continuation at depth of the San Román backthrust (Figure 7, CL2) is revealed by south dipping reflective facies of the Peraltilla and Sariñena Fms., which are detached along BFm4 evaporites. Reflectors and the backthrust are slightly folded by a deeper-seated and south directed thrust system detached along the base of BFm1. Like in CL1, the San Román backthrust roots in the southern tip point of a south directed thrust detached along the base of BFm4 that connects with the SPST. A close look around the tip point (Figure 7, CL2, detail) demonstrates that this detachment level thins close to the hanging wall inflection point (i.e., the tip point) and suggests salt evacuation from a mobile detachment.

5.2.3. Seismic Composite Lines-3 and 4; Barbastro Anticline and Sierras Transition Zone

West of the STZ, the Costeán thrust sheet and Naval anticline are fossilized by the STZ unconformity which is, in its turn, truncated by the Naval thrust (Figure 7, CL3). The Salas thrust sheet shows a hanging wall anticline folding the base of Middle-Upper Eocene units which suggests its lateral termination eastward (Figure 7, CL3). The described system is unconformably topped by the Oligo-Miocene, flat-lying reflectors. The SPST is detached along BFm3 and describes a horizontal to north dipping geometry from north to south.

Field observations west of Barbastro village (Figure 3) evidence a north verging thrust of the Barbastro Fm. over the Sariñena Fm., where alluvial sediments, interbedded within the Barbastro Fm., define an overturned forelimb (Barnolas, García-Sansegundo, & Teixell, 1990). A gravity high extends into the outcropping evaporites (Figure 5), suggesting the presence of a denser body underneath, likely the footwall of the north-verging thrust. These evidences together with few isolated and discontinuous reflectors within transparent to chaotic seismic facies helped us to interpret the Barbastro anticline as a duplex system featuring up to three foreland-verging thrusts detached along the base of BFm1 and up to two hinterland-verging passive roof thrusts detached along BFm3 or BFm4 (Figure 7, CL3 and CL4). Hence, the floor sequence involves the BFm1 and two subunits and the roof sequence, decoupled along the BFm3 and four subunits, groups the BFm3 and four detachments and the Peraltilla and Sariñena Fms.

South of the Barbastro anticline, Triassic to Jurassic rocks overlie the basement and gradually disappear to the north under the Ebro erosional unconformity which is overlain by the Ebro Basin autochthonous succession. Seventeen kilometers south of the Barbastro anticline, the Peralta de Alcofea anticline (Figure 3) arises as a gentle fold related to the tip point of a flat-lying blind thrust (Peralta de Alcofea blind thrust) detached along the base of BFm3 (Figure 7, CL3 and CL4). In between both anticlines, a 6–7 km wide, gentle syncline sinks into the BFm3 subunit. This evaporitic subunit accommodates folding by a [c]40% thinning (Figure 7, CL4, detail). Again, suggesting outward migration of evaporites.

5.2.4. Seismic Line HL-7; Barbastro Anticline and Azanuy Syncline

Following the interpretation by Sans et al. (1996), the Barbastro anticline is a south directed, BFm1-detached, duplex system with antiformal geometry and involves a floor sequence most likely consisting of BFm1 and 2 (Figure 7, HL-7). The uppermost thrusts detach along BFm3. Toward the hinge of the antiform, in its front, this thrust is folded. This is evidenced by downward facing hanging wall folds which are truncated by a hinterland-verging thrust underlying the southern limb of the Barbastro anticline. The interpreted thrust stacking and north directed backthrusting is compatible with a duplex geometry involving foreland-verging duplexing and hinterland-verging thrusting as observed in our western sections. To the north, the gentle, symmetric Azanuy syncline shows a northern limb which is affected by a hinterland-verging thrust and truncated by a south directed thrust system (Figures 3 and 7). Below the

Azanuy syncline, south directed thrusts describe a flat geometry. Conversely to western transects, the deformation in the Ebro Basin is localized in two locations; the Barbastro anticline to the south of the Azanuy syncline and the northern thrust system to the north (Figure 7, HL-7).

6. Main Structural Features in Map View and 3-D

Seismic coverage allows the construction of key surfaces based on the interpolation of discrete horizons. Key modeled surfaces are relatively large, thus guaranteeing a reliable lateral continuation and profile to profile correlation. We have considered a total of 13 surfaces: seven of them are stratigraphic contacts (tops of the basement, BFm2, BFm3, BFm4, and Peraltila Fm., and the Ebro and STZ unconformities) and the other six tectonic structures (the San Román and Barbastro anticline main backthrusts, the SPST and Alcanadre, Salas, Balzes, and Costeán thrusts). Surface interpolation was performed using the Move software package (by Midland Valley & Petroleum Experts). From west to east and north to south, the Barbastro Fm. seismic subunits thin and shallow. BFm1 varies from more than 1,400 m below the Gavarnie-Sierras thrust sheets and disappears to the southeast of the studied area. From west to east, BFm2 and BFm4 thins from 280 to 120 m and 250 to 100 m, respectively. As an exception, BFm3 shows a trendless variation between 300 and 450 m. South of the Barbastro anticline and from west to east, the top of BFm1, BFm2, BFm3, and BFm4 shallow from $-2,850$ to $-1,675$ m, $-2,560$ to $-1,540$ m, $-2,180$ to $1,150$ m, and $-1,930$ to $1,050$ m, respectively.

6.1. The Western Termination of the South Pyrenean Triangle Zone

The seismic interpretation of our case study shares some of the inherent uncertainties found in other triangle zones and salt related structures: for example, poorly reflective facies, seismic artifacts such as pull-ups and pull-downs (Figure 7, CL2 and CL3, respectively), shadow areas (Jardin et al., 2007; Jones & Davison, 2014; von Hagke & Malz, 2018), and time-to-depth conversion misfits against true depths. These drawbacks result from the structural style within the triangle zone (stacked thrusts and steeply dipping strata and faults) and the heterogeneity of the Barbastro Fm. The hinterland verging thrust of the eastern sector (Figure 7, CL1) is well imaged and our interpretation agrees with previous works (e.g., Martínez-Peña, 1991; McElroy, 1990; Millán, 1996). However, the central sector, where evaporitic content and structural complexity increases, is not fully imaged in seismic lines. Conversely, our interpretation is enriched by evidence coming from field and gravity data and conceptual structural models. For example, the innermost hinterland-verging backthrust crops out to the east of the central sector and its continuation at depth is explained by a gravity high related to presence of the SPST as its footwall. Although the quality of seismic profiles does not allow an unequivocal interpretation of the target structure, these elements led us to interpret the Barbastro anticline as a duplex system.

To illustrate the termination of the triangle zone, six serial cross sections (see Figure 8a for location) were built based on the interpolated surfaces and on the interpretation of surface geology, seismic and well data. These cross sections highlight along-strike changes in the geometry of the Barbastro anticline and San Román backthrust (Figure 8b). North of the easternmost section (Figure 8b, A), the deformation concentrates (i) in a foreland-verging thrust system that links with a hinterland-verging thrust and, to the south, (ii) in an antiformal stack depicting hinterland-directed thrusts at the front. These structures change laterally to a foreland-verging, floor duplex system decoupled from a hinterland-verging roof duplex system. These floor and roof duplexes link at their southern tip. North of these duplexes, the SPST is buried below the STZ unconformity and backthrusted (Figure 8b, B and C) or, alternatively, it is folded and exhumed (Figure 8b, D). To the west, the south directed floor sequence duplex is reduced to a single thrust and a related gentle hanging wall anticline (Figure 8b, E) which indicates the lateral termination of the duplex system and the transition to the San Román backthrust (Figure 8b, E). Farther west, the San Román backthrust grades into a hinterland-verging thrust and a fault-propagation fold (Figure 8b, F) which is finally reduced to a residual structure near its tip point.

Geometrically, the Barbastro anticline duplex system can be ascribed to a ramp-dominated, multiple triangle zone (see section 8) whereas the San Román backthrust represents the hinterland-verging thrust of a detachment-dominated triangle zone (von Hagke & Malz, 2018). Approximately 60 km along strike, this structural gradation represents the transition from a ramp to a detachment-dominated triangle zone and the lateral termination of the latter (Figure 8). South of the Barbastro anticline, the Peralta de Alcofea

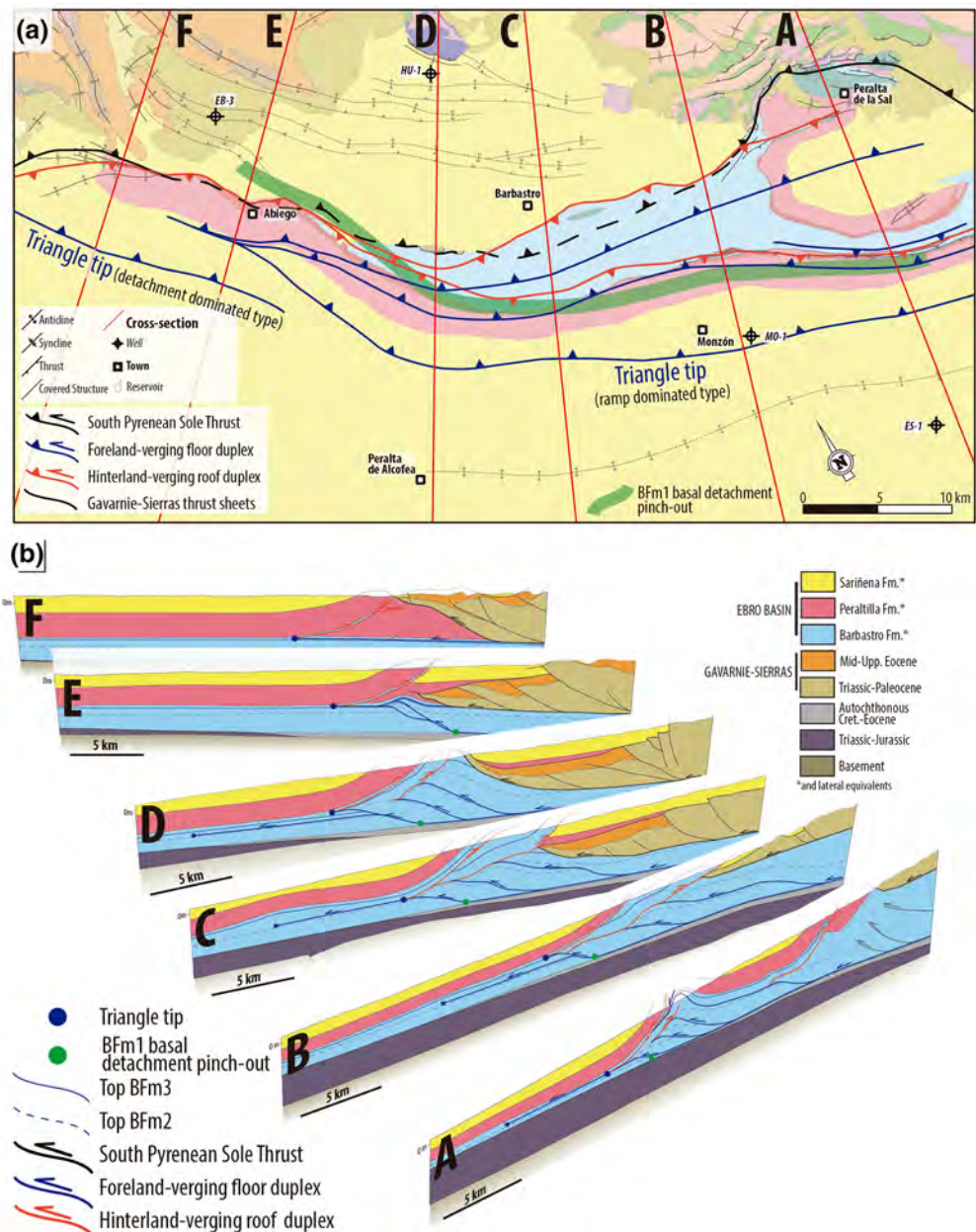


Figure 8. (a) Ebro Basin key structural traces: Blue lines represent the intersection of the south directed floor sequence thrust with the north directed roof sequence duplex backthrusts (red lines). (b) Serial cross sections of the western termination of the South Pyrenean triangle zone. Black-, blue- and red-lined structures correspond to the South Pyrenean Sole Thrust, the foreland-verging and the hinterland verging duplexes, respectively.

anticline is defined as a detachment fold that can be interpreted as an incipient pop-up structure (in the sense of Butler, 1982) associated with the Barbastro anticline duplex system. This structure runs parallel to the southern flank of the Barbastro anticline and extends, at least, 3–4 km.

In the studied area, the deformation in the Ebro Basin extends from the tip of the triangle zone to the SPFT (Figure 8a) and mimics its salient and reentrants geometry. Therefore, the deformed area is 15 km wide and it narrows to the west, as the SPFT extends to the south along the front of the STZ. The base of BfM1 represents its lower boundary. Toward its western termination, it narrows to a 7 km wide area whose southern limit coincides with the San Román backthrust tip line (Figure 8a). In this case, the lower boundary is represented by the BfM4 detachment rather than the BfM1 one as it happens to the east.

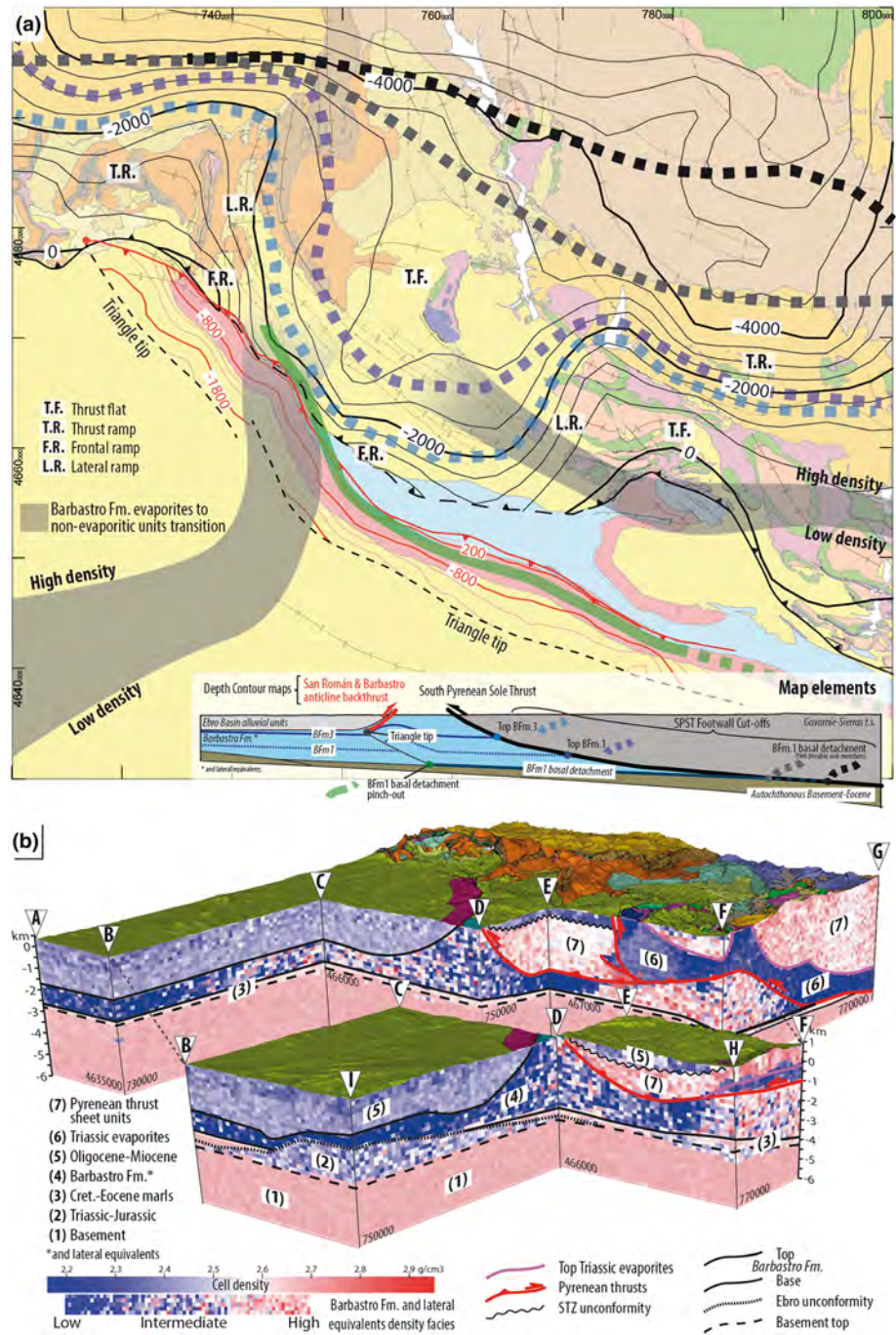


Figure 9. (a) The structural meaning of the following map elements is detailed in the synthetic section at the bottom of the map. The depth contour maps of the South Pyrenean Sole Thrust and the San Román and Barbastro anticline outermost backthrust are displayed together with geological map at the background. Solid thick green line corresponds to the location of the BFm1 basal detachment, the tens to hundred-meter thick basal detachment in this area of the Ebro Basin. Dashed thick lines represent the SPST footwall cutoffs of the top of BFm1 (light blue), BFm3 (dark blue), and the BFm1 basal detachment (dark gray and black; two end-member cutoff possibilities after from Muñoz et al., 2018). Gray-shaded areas represent the density transition between low-density rocks (evaporites, southeast) to higher density rocks (detrital, west, and north) through the Barbastro Fm. and lateral equivalents. This density transition has been extracted from the gravity inversion voxel showed in (b). (b) Three-dimensional view of the density voxel resulting from the gravity inversion where key horizons and structures are digitalized. Number labels correspond to gravity modeled units (Units 1 to 5 are similar to seismic facies units). Letter labels are used to localize voxel sections referred to in the text.

6.2. The South Pyrenean Sole Thrust and the Gavarnie-Sierras Thrust Sheet

Aiming to integrate most of these results in map view, we contoured the geometry at depth of the SPST (Figure 9a). To the east, the SPST exhibits a 10 km wide thrust flat (Marginal Sierras Unit) that steepens up to 30° to the north. To the west, the SPST gradually deepens and forms a 23 km wide convex thrust flat along the STZ. Its front is characterized by a 7 km band parallel to the Barbastro anticline where the SPST shallows and steepens up to 60° to the north (Figure 8b, D). West of the STZ thrust flat, a N-S trending lateral ramp with a depth offset of about 1.5–2 km marks the transition toward the External Sierras. There, the SPST depicts an E-W trending, 25° northward dipping, regular thrust ramp (Figure 9a).

Rooted on the SPST, the External Sierras thrust sheets plunge into the STZ conglomerates and either merge the SPST thrust (Alcanadre thrust sheet) or continue eastward. For example, the Balzes thrust sheet progressively dies out and is relayed by the Costeán thrust sheet while the Salas thrust sheet extends further east and splays into two minor thrusts (Figure 3). Structural wavelength varies laterally along the STZ from 2–3 km in the west to 4.5–5.5 km to the east and it decreases again in the Marginal Sierras (Figure 3).

7. Gravity Inversion: Facies Distribution in the Barbastro Fm. and Laterally Equivalent Units

Gravity inversion was focused on modeling the 3-D density distribution of the Barbastro Fm. and laterally equivalent units. The output result is a voxel (Figure 9b) where each cell is defined by a constant density resulting from the inversion. The density variations within the Barbastro Fm. and equivalent units show low-, medium-, and high-density facies (blue to red, Figure 9b) that correlate with evaporites, evaporitic and marly-sandy facies and marls-sands to conglomerates, respectively. Thus, the following description focuses on the density distribution within Barbastro Fm. and lateral equivalents, our main target (Unit 4, Figure 9b).

To the south (Figure 9b, A-B and B-I sections), low-density values point to a main evaporite composition of the Barbastro Fm. From B to C, density grades from low (2.2–2.35 g/cm³) to intermediate values (2.35–2.5 g/cm³). Medium-density values continue to the east (Figure 9b, C-D section) as they approach the core of the Barbastro anticline. D-E section displays a progressive intermediate-to-low-density transition, whereas E-F section shows a rapid change from low- to high-density values (2.5–2.7 g/cm³) that continues to the north in section F-G. To the east (section H-D), the Barbastro anticline core features a subtle transition from low- to intermediate-density values. This density distribution grades abruptly to the east (section D-H) where it passes to high-density values that extend to the north (section H-F).

Based on these density variations and considering the density to lithology equivalences, we were able to construct a map depicting the lithological transition between the Barbastro Fm. evaporites (low density) and its lateral detrital equivalents (high density) (Figure 9a, gray bands). Broadly, the evaporites dominate in the southeastern sector, coinciding with the Barbastro anticline and the Ebro Basin to the south. Along the eastern sector, the low- to high-density transition shows a N090°E to N110°E trend, which coincides with the transition between evaporite to terrigenous facies north of the Azanuy syncline (Senz & Zamorano, 1992) and helps to validate the applied technique based on gravity inversion. From the western limit to the east, transition occurs along a N080°E trending area that takes a N-S orientation. This one coincides with the end of the outcrop of the Barbastro Fm. evaporites, and the transition between the Barbastro anticline and the San Román backthrust. Besides, it is aligned with the N-S lateral ramp of the SPST. Connection between western and eastern facies transitions is obscured by the accumulation of Triassic evaporites coring the Balzes anticline (Figure 9a).

8. Discussion

8.1. The Mechanical Stratigraphy of the Barbastro Fm. and Lateral Equivalents: A Multidetachment Evaporitic Unit

The Barbastro Fm. has been described as an evaporite-rich unit. However, our results indicate that it did not behave as a décollement unit prone to undergo a significant amount of diapiric accumulation as interpreted previously (Almela, 1965; Martínez-Peña & Pocoví, 1988; Riba & Llamas, 1962; Ríos, 1948). It can be rather considered as a multidetachment unit where low-strength detachment subunits localized deformation.

Contractional structures systematically detached along the base of BFm1 (regional glide horizon for the Barbastro anticline duplex system), BFm1 itself (detachment horizon for the STZ thrust units), BFm3, and the base of BFm4 (Figures 7 and 9a). These subunits consist of pure halite, and a mix of halite, anhydrite, and mudstones (Gil & Jurado, 1998), and massive gypsum [MO-1 well]. In addition to acting as fault gliding horizons, BFm3 and BFm4 show some evidence of thinning-thickening trends that suggest restricted evaporite migration (Figure 7, details in CL2 and 4, Gil & Jurado, 1998). In the Barbastro anticline and southward, field observations, well log lithological descriptions and the gravity inversion suggest that these detachments are interbedded with low to medium density rocks such as evaporites and shales (Figure 9b). North of the N120°E trending density transition (Figure 9a), gravity inversion suggests that the evaporitic content considerably diminishes (Figure 9). Therefore, evaporitic detachments appear interbedded with rocks of higher density (mainly sandstones and mudstones) (Figure 9b). The spatial distribution of these detachments defines the mechanical stratigraphy of the system, which controlled the structural and kinematic evolution of the triangle zone and the Gavarnie-Sierras thrust sheet (see section 8.3).

In the southern sector of the studied area, the base of BFm1 grades from a 100 m thick level of halite and gypsum [HU-1 well] into a carbonate-mudstone succession with interbedded sandstones, limestones, and anhydrite nodules (Gil & Jurado, 1998) [MO-1 & ES-1 wells]. This gradation suggests that the salt-rich detachment pinches out in this area. Being aware that this facies change is gradual and the transition area can expand from 2 to 50 km (Arenas & Pardo, 1999; Ezquerro, 2017), we suggest that the pinch-out of this halite-based detachment is most likely located at the base of the outermost ramp that defines the triangle zone (Figure 9a). This hypothesis implicitly considers that this pinch-out controlled the location of the flat to ramp thrust transition, as observed to the east of the South Pyrenean triangle zone (Sans et al., 1996). The BFm1 basal detachment extends from this southern pinch-out to its structural truncation represented by the autochthonous Upper Eocene cutoff lines proposed by Muñoz et al. (2018) (Figure 9a). The base of BFm1 acted as a regional detachment, eventually interpreted as the Cardona Fm., for the Pyrenean triangle zone in the studied area and further east (Muñoz et al., 2018; Sans et al., 1996; Senz & Zamorano, 1992). Cutoff relations between BFm1 and BFm3 and the geometry of the SPST indicate that the Gavarnie-Sierras thrust sheet detached along BFm1 as a whole (not necessarily its base) describing a thrust flat along the STZ. Laterally, from east to west, BFm1 may present a N-S incompetent to competent mechanical transition controlling the location of the lateral ramp between the STZ and the External Sierras Unit (Figure 9a). This transition may coincide with the northern continuation of the N-S, low- to high-density transition defined from gravity inversion in the Ebro Basin (Figure 9a).

Shallower detachment subunits (BFm3 and 4) extend farther south, beyond the tip line of the Barbastro anticline duplex system, as evidenced by: (i) the presence of evaporites (mainly halite) which can represent more than 50% of the lithological content of these subunits in the southernmost wells [SA-1 and ES-1] (Gil & Jurado, 1998; Lanaja, 1987) and (ii) the occurrence of the Peralta de Alcofea anticline, linked to thickening-thinning of salt levels (Figure 7). In the STZ, their continuation toward the north is uncertain because shallower detachments are truncated by the SPST (Figure 9a). Along the central and eastern sectors, BFm3 represents a weak, glide horizon along which both the Gavarnie-Sierras thrust sheet and the Peralta de Alcofea blind forethrust detached. Only the BFm4 detachment extends westward beyond the low to high, N-S density transition (Figure 9a).

8.2. Time Constraints on the Gavarnie-Sierras Thrust Sheet and the Barbastro Duplex System Evolution

The Gavarnie-Sierras thrust sheet underwent a period of folding and thrusting together with vertical axis rotation during the Middle-Late Eocene (McElroy, 1990; Millán, 1996; Millán-Garrido et al., 2000; Mochales et al., 2012; Muñoz et al., 2013; Nichols, 1987; Oliva-Urcia et al., 2019; Oliva-Urcia & Pueyo, 2007; Poblet et al., 1998; Pueyo et al., 1997; Puigdefàbregas, 1975; Rodríguez-Pintó et al., 2016). At the STZ, however, this event is difficult to analyze because neither the description of lithological logs from well data nor the resolution of seismic reflection profiles are detailed enough to distinguish between Middle and Upper Eocene units. The composite lines shown in this work highlight the occurrence of growth strata, onlap relationships, and erosional truncations possibly related to this deformation event (Figure 7, CL2, 3, 4). Unfortunately, reliable timing constraints are not widely recognizable and, besides, their lateral continuity is sometimes doubtful. From seismic profiles, interpreted relative timing evidences suggest that frontal

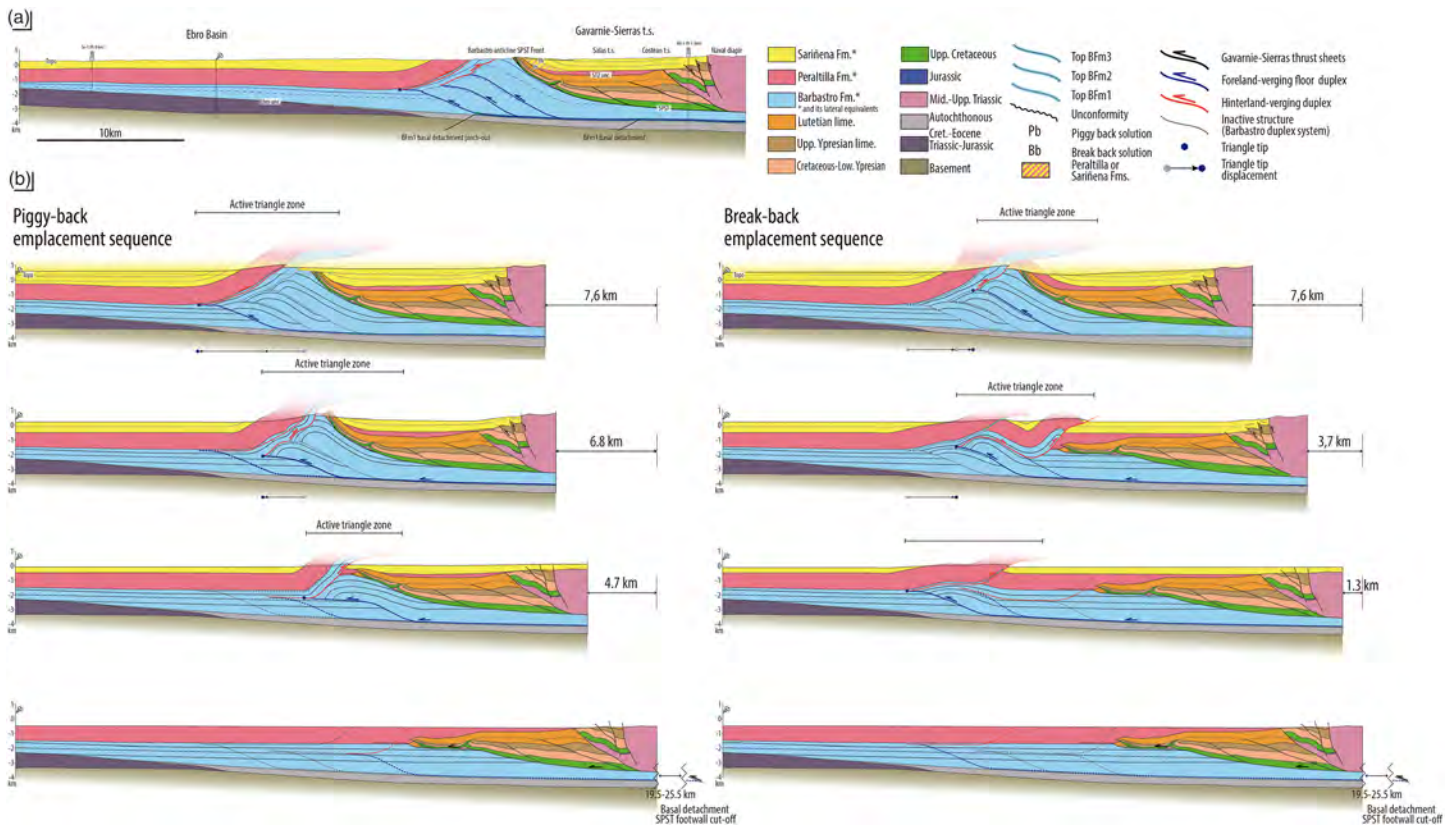


Figure 10. Evolutionary reconstruction of the formation of the Barbastro anticline duplex system illustrated by (a) cross section D (Figure 8 for location) and (b) two restoration solutions. It is worth mentioning that the distinction between the Peraltilla and Sariñena Fms. in the Gavarnie-Sierras is done after restoration, and both solutions are displayed and labeled as Pb (Piggyback) and Bb (Break-back) solutions. In the STZ, below the Sariñena Fm., seismic imaging does not allow to differentiate these Oligocene-Miocene units (Figure 7).

thrusts and folds were relatively short-lived structures developed during the Early-Middle Eocene and subsequently fossilized, as evidenced by the continuity of reflectors above the STZ unconformity (Oligocene in age, Figure 7, CL3–5). These reflectors are truncated by inner thrusts meaning either that these structures were active from Early-Middle Eocene to the Oligocene or that they were emplaced according to a hanging wall sequence or reactivated out-of-sequence during the Oligocene.

Subsequently, the Gavarnie-Sierras thrust sheet detached and moved southward. The SPST main southward displacement event postdates the deposition of the Barbastro Fm., that was clearly overthrust. In addition, the Peraltilla Fm. is the youngest unit overthrust by the SPST. This thrust was fossilized by the STZ unconformity during the latest Rupelian. All in all, the main event of southward displacement on the SPST can be bracketed between the Rupelian and the Early Chattian and is therefore partly coeval with the deposition of the Peraltilla Fm. (Figure 10, see also Senz & Zamorano, 1992). The Gavarnie-Sierras thrust sheet detached along the Triassic evaporites, whose southern pinch-out might have governed the location of the frontal cut-off of the SPST. Nevertheless, the emplacement of this thrust sheet was largely controlled by the Barbastro Fm. detachments. Weak detachments favored the formation of a thrust salient and thrust flat geometries, as it occurs in the STZ. Conversely, their lateral transition to more competent lithologies promote the formation of thrust reentrants in the Marginal and External Sierras.

Synchronously to the deposition of the Sariñena Fm. (Chattian to Aquitanian), most of the shortening was transferred from the lower detachment level (Triassic evaporites) to the upper one (Barbastro Fm. and lateral equivalents) and accommodated by the Barbastro anticline duplex system and the San Román backthrust. Their coeval activity is evidenced by the Sariñena Fm. which is unconformably overlying the Peraltilla Fm. at the western termination of the Barbastro anticline and along its northern limb (Luzón, 2005). The basal blind thrust that connects the SPST and the San Román backthrust is gently folded by the lateral

termination of the floor duplex sequence and hence backthrusting may predate or be coeval to the emplacement and the activation of the floor detachment (base of BFm1). It is worth noticing that the Barbastro Fm. and its equivalents favored the emplacement of the Gavarnie-Sierras thrust sheet during Late Eocene–Oligocene times whereas the basal detachment activated afterward (Figure 10). The activation of the basal detachment triggered the formation of the Barbastro anticline duplex system which is likely related to the emplacement of the youngest basement thrust, north of the study area (i.e., Guarga basement thrust, Early Chattian to Aquitanian; Millán Garrido et al., 2006), that is recorded in the External Sierras (Labaume et al., 2016) and in the Marginal Sierras (Millán-Garrido et al., 2000; Santolaria et al., 2015).

8.3. Origin and Growth of the Western Termination of the South Pyrenean Triangle Zone

The origin of the Barbastro anticline has been related to different salt tectonics processes, such as diapiric thickening (Martínez-Peña & Pocoví, 1988), buoyancy, and differential loading, combined with thrusting (Gil & Jurado, 1998) and expressed as an antiformal stack (Sans et al., 1996) or as a detachment fold (Barnolas, García-Sansegundo, & Teixell, 1990; García-Sansegundo et al., 1991). Our interpretation gives more weight to thrust stacking by duplexing than pure diapirism. However, a component of buckling or salt accumulation cannot be completely discarded as evidenced by the numerous, vertical-axis folds found in the outcropping Barbastro Fm. (Senz & Zamorano, 1992) and the salt migration processes inferred from seismic lines (Figure 7, details in CL2 and 4).

The Barbastro anticline duplex system and the San Roman backthrust represent a good example of how deformation evolves laterally in a triangle zone termination. In this case, a well-developed multidetachment duplex system interpreted as a ramp-dominated, multiple triangle zone type grades laterally into a detachment-dominated triangle zone (von Hagke & Malz, 2018) (Figure 8), which dies out in a fault-propagation fold.

The restoration of the triangle zone (Figure 10) can be done according to two end-member solutions with different mechanical implications: piggy-back or break-back emplacement sequences (Figure 10). Intermediate solutions are also feasible, and would include oscillating sequences (Smit et al., 2003), out-of-sequence thrusting or coeval thrust activity. A common feature of earlier interpretations of the Barbastro anticline, that we also incorporate, is that deformation was channelized through a detachment directly overlying the Ebro Eocene marls, that is, the base of BFm1. Then, the basal, south directed, flat-lying thrust detached along BFm1 and ramped up as it encountered a mechanically weaker Ebro Basin cover (piggy-back emplacement sequence solution) or the outer pinch-out of the basal detachment (break-back emplacement sequence solution) (Figure 10). In the first case, the basal thrust ramped up and ended in the BFm3 level (7.5 km ahead of the SPFT), where it linked to a hinterland verging (passive) roof thrust. This defined a first triangle zone. Newly formed forethrust and backthrust (i.e., new triangle zones) led to the foreland propagation of the triangle tip. Regarding the break-back sequence solution, the southernmost triangle zone predated the formation of the inner duplex system. In this solution, the formation of backthrusts took place behind the leading edge of deformation. Within this framework, the outermost gentle anticline (Peralta de Alcofea anticline, Figures 3 and 7) can be interpreted as an incipient (piggy-back sequence solution) or unsuccessful (break-back sequence solution) pop-up structure related to the frontal triangle zone.

In both solutions (and in intermediate ones) shortening accommodated by the foreland-verging floor duplex must have a counterpart in hinterland-verging thrusting in the roof duplex sequence. The localization of deformation at the tip of the basal décollement can be explained by the mechanical stratigraphy and/or the southward decrease of the effective thickness of the décollement. This would explain the location of the Barbastro anticline and its geometry, that is probably parallel to the shoreline of the evaporitic lakes formed in the foreland basin beyond the SPST front. The delamination of the Ebro Basin sequence, and consequently the formation of the triangle zone, would be favored by halite-based, low-strength shallow detachments. The nearly horizontal disposition and the low friction of these roof detachments entailed a nonpreferential structural vergence situation (Davis & Engelder, 1985) that could promote underthrusting (Jamison, 1993).

Mechanical constraints involved in the occurrence and evolution of backthrusts in Mohr-Coulomb wedges (see, e.g., Buitier, 2012; Dahlen et al., 1984; Dean et al., 2013; Hilley & Strecker, 2004) can provide a frame for

testing some of the features of the proposed models. According to the critical taper theory under Mohr-Coulomb behavior, in a simple approximation the square of the width of the wedge is proportional to shortening and to the thickness of the involved (deformed) layer and inversely proportional to the opening angle of the wedge (Dahlen, 1990). The width of the foreland wedge associated with the Barbastro anticline ranges between 7.5 and 9.5 km, and the thickness of the thickened unit (that can be considered to build the wedge) is 2 km. Having these figures in mind, the wedge opening angle should be about 21–30°, a high value (at the limits of stable configurations, see Buiter, 2012) when compared with standard values obtained for orogenic belts and accretionary prisms but consistent with the geometry obtained from cross sections.

On the other hand, if we apply the critical taper equation (see, e.g., Davis et al., 1983; Suppe, 2007) a very low taper angle is expected in salt detached systems with a very low basal friction (Davis & Engelder, 1985), as it is expected in our case, regarding the evaporite composition of the Ebro Basin detachments. We consider here that for subaerial wedges the term $[1 - (\rho_f/\rho)]$ can be equaled to 1, because the fluid (air) density over rock density is negligible. The apparent contradiction between the actual values obtained (21–30°) and the very low taper angles estimated from the critical taper equation (Davis et al., 1983) can be related to (1) an unexpected, evaporite-based, strong detachment (or a weaker brittle wedge, Suppe, 2007). Or (2) the above-invoked transition from a weak to a frictional basal décollement, that would allow the increase of the wedge slope angle. In both cases, hypothetical gravitational spreading of the wedge (Mourgues et al., 2014) would be prevented by its intracutaneous development (see, e.g., Poblet & Lisle, 2011).

In the two proposed end-member evolutionary models (piggy-back and break-back sequences, Figure 10) the blocking of the earlier frontal thrust had important consequences in the evolution of the thrust sequence, but the reason for the triggering of subsequent thrusts is completely different, from the mechanical point of view, in both models. In the piggy-back sequence model, the first formed thrust was probably blocked by the steep dip of the backthrust limiting the triangle zone. This makes its reactivation difficult for standard values of friction coefficients (Byerlee, 1978) and favors the development of forethrusts in the footwall, thus defining the self-similar growth of the wedge. The shallow dip of forethrusts (25°) is controlled by the low friction angle (in average) of the unit, particularly, of its basal thrust: angle of $45^\circ - f/2$ between fractures and the sub-horizontal s_1 axis, taking into account a low-strength décollement and a low deformation rate. This rate can be roughly estimated in 0.5 mm/year in average (displacement of 8 km during a time span between the Rupelian and Aquitanian, Puigdefàbregas et al., 1992; Vergés et al., 1992). A more accurate dating of the syn-tectonic series based on magnetostratigraphic will shed some light on this issue. In the break-back model mechanical constraints are similar, with the difference that the blocking of the earlier thrust would result in the development of thrusts in its hangingwall, that in their turn, would be blocked because of the steep dip of their forelimbs against the southern margin of the triangle zone. Nevertheless, in both cases an important factor that must be taken into account is that the steep dip of the backthrusts limiting southward the triangle zone is not conditioned by the original dip of foreland-dipping fractures (that would be meaningless in this scenario) but rather by the dip of the forelimb of the floor sequence duplexes. Large-scale analogs of this kind of geometrical features can also be found at the tip of basement-involved mountain ranges (Brocher et al., 2004; Turienzo et al., 2020).

On the other hand, erosion could have contributed to keep the orogenic wedge under subcritical conditions in the triangle zone (see, e.g., Konstantinovskaya & Malavieille, 2011, and references therein). Erosion toward the Ebro Basin contributed to maintain the movement of the hinterland verging roof thrusts (without actual mass transfer, for what erosion of the hangingwall was a much more effective process) by lowering the upper slope angle of the tectonic wedge (see, e.g., DeCelles & Mitra, 1995) and sustain the development of the triangle zone (Mugnier et al., 1997). Conversely, limited aggradation by sedimentation on top of the wedge did not probably have much influence in its evolution.

Results from analog modeling embrace both solutions. A common observation in salt detached system models is that deformation nucleates, at some point during the modeling, in the outer pinch-out of the ductile horizon and that there is not a systematic fold-and-thrust emplacement sequence (Costa & Vendeville, 2002; Santolaria, Vendeville, et al., 2015; Smit et al., 2003; among others). Along the eastern sector (HL-7 seismic section, Figure 7), where tectonic activity is registered in the Azanuy syncline, Senz and Zamorano (1992) concluded that the deformation in the Ebro Basin satisfies a piggy-back emplacement sequence which could be extrapolated to the analyzed cross section.

9. Conclusions

A combined and integrated workflow including the interpretation of seismic reflection profiles supported by surface geology and exploration well data together with the interpretation of the gravity anomalies and 3-D stochastic inversion has proven to be a powerful approach to study deformed multidetachment evaporitic units and specifically the western termination of the South Pyrenean triangle zone. In the South Pyrenean triangle zone, density contrasts between the Eocene and Triassic evaporitic units and nonevaporitic rocks, from the Paleozoic basement to Oligocene alluvial rocks, makes the gravity prospecting and modeling a suitable approach which is here used to delineate the changes in the subsurface distribution of lower density facies (i.e., evaporitic subunits) within the Barbastro Fm. In particular, the 3-D stochastic inversion of the gravity data, has been useful to understand the 3-D density variations of low-density (salt) units and their implications in the overall geometry and the related changes in the structural style and may have a wider applicability in other regions if a significant contrast in the density of the involved rocks is observed.

In the Ebro Basin, the Barbastro anticline is here interpreted as a ramp-dominated, multiple-triangle zone detached along a halite-based gliding horizon at the base of the Ebro Basin autochthonous Barbastro Fm. Still in this multidetachment unit, shallower detachments favored the delamination of the cover and the decoupling of the floor and roof duplex systems. The duplex system progressively disappears to the west as the evaporitic content dramatically diminishes as evidenced by facies modeling derived from gravity inversion. The Barbastro anticline connects with the San Román backthrust to the west. This structure represents the hinterland-verging thrust of a detachment-dominated triangle zone. All in all, the western termination of the South Pyrenean triangle zone is defined as the transition from a ramp-dominated, multiple-triangle zone to a detachment-dominated triangle zone that dies out to the west.

Apart from the impact in the Ebro Basin deformation, the 3-D distribution of the detachment unit exerted a significant control on the structural style and kinematics of Pyrenean structures, represented by the Gavarnie-Sierras thrust sheet. Distribution of detachment units influenced the location of thrust salients and reentrants, structural spacing, and geometry.

Data Availability Statement

Data sets (seismic profiles as tiff files, well, density, and gravity data) for this research are available in the SIGEOF repository, the Geophysical Information System of the IGME (Spanish Geological Survey). To access the data, use the web application (info.igme.es/SIGEOF/). To visualize and request the data, choose the wanted data set in the drop down menus and perform an areal search with the following bounding limits, in geographical coordinates: N: 42.4932; S: 41.7653; W: -0.3503; E: 0.6676. The work identifiers for the data collected during the aforementioned projects are “8700” and “8900,” for DR3AM and “8600” and “8800” (gravity and petrophysics, respectively), for KINESAL. The data are available under request and free of charge. The license information is found in this site (http://info.igme.es/SIGEOF/doc/LICENCIA_USO_IGME_EN.pdf). For further information, see this site (<http://info.igme.es/SIGEOF/doc/ManualSIGEOF.pdf>).

References

- Almela, A. (1965). Tectónica Yesífera de la Cuenca del Ebro. In *I Coloquio Internacional sobre las Obras Públicas en los Terrenos Yesíferos* (pp. 5–11). Madrid.
- Anadón, P., Cabrera, L., Coldeforns, B., & Sáez, A. (1989). Los sistemas lacustres del Eoceno superior y Oligoceno del sector oriental de la Cuenca del Ebro. *Acta Geologica Hispánica*, *24*(3–4), 205–230.
- Anderssen, R. S., & Seneta, E. (1971). A simple statistical estimation procedure for Monte Carlo inversion in geophysics. *Pure and Applied Geophysics*, *91*(1), 5–13. <https://doi.org/10.1007/BF00879552>
- Anderssen, R. S., Worthington, M. H., & Cleary, J. R. (1972). Density modelling by Monte Carlo inversion—I Methodology. *Geophysical Journal International*, *29*(4), 433–444. <https://doi.org/10.1111/j.1365-246X.1972.tb06169.x>
- Arenas, C., & Pardo, G. (1999). Latest Oligocene–Late Miocene lacustrine systems of the north-central part of the Ebro Basin (Spain): Sedimentary facies model and palaeogeographic synthesis. *Palaeogeography Palaeoclimatology Palaeoecology*, *151*(1–3), 127–148. [https://doi.org/10.1016/S0031-0182\(99\)00025-5](https://doi.org/10.1016/S0031-0182(99)00025-5)
- Ayala, C., Bohoyo, F., Maestro, A., Reguera, M. I., Torné, M., Rubio, F., et al. (2016). Updated Bouguer anomalies of the Iberian Peninsula: A new perspective to interpret the regional geology. *Journal of Maps*, *12*. <https://doi.org/10.1080/17445647.2015.1126538>
- Banks, C. J., & Warburton, J. (1986). “Passive-roof” duplex geometry in the frontal structures of the Kirthar and Sulaiman mountain belts, Pakistan. *Journal of Structural Geology*, *8*(3–4), 229–237. [https://doi.org/10.1016/0191-8141\(86\)90045-3](https://doi.org/10.1016/0191-8141(86)90045-3)
- Barnolas, A., García Senz, J., Zamorano, M., Montes, M., & Rico, M. (1990). *Mapa Geológico de España. 1:50000, Hoja 326, Monzón*. Madrid: IGME.

Acknowledgments

This work was financed by the DR3AM (CGL2014-54118-C2-2-R) and E-28 (GeoApp Research Group) projects by the Spanish Ministry of Science and the Aragón Government, respectively. This work has received support from and it also aligns with methodological goals of the GeoERA project 3DGeoEU (ERANET Cofund action 731166 [H2020], Project code GeoE.171.005) and GeoPiri3D project (from the Spanish Ministry of Education and Universities, project code CGL2017-84901-C2-2-P). We acknowledge the TopoIberia project for providing the gravity data from SITPOPO databases. The Academic agreement with MVE is also acknowledged. The IHS is also acknowledged for providing the Kingdom Suite software. José María Llorente and Agustín González are here acknowledged for gravity data acquisition and processing. We also want to thank reviewers Christoph v. Hagke and Jonas Kley and Editor Laurent Jovilet for their productive suggestions and comments that helped to enrich our work and improve the manuscript.

- Barnolas, A., García-Sansegundo, J., & Teixell, A. (1990). *Mapa Geológico de España. 1:50000, Hoja 287, Barbastró*. Madrid: IGME.
- Barnolas, A., Teixell, A., García Senz, J., & Ramirez, J. I. (1990). *Mapa Geológico de España. 1:50000, Hoja 288, Fonz*. Madrid: IGME.
- Barnolas, A., Teixell, A., Zamorano, M., & Ramirez, J. I. (1994). *Mapa Geológico de España. 1:50000, Hoja 250, Graus*. Madrid: IGME.
- Bonini, M. (2001). Passive roof thrusting and forelandward fold propagation in scaled brittle-ductile physical models of thrust wedges. *Journal of Geophysical Research*, *106*(B2), 2291–2311. <https://doi.org/10.1029/2000JB900310>
- Borderie, S., Graveleau, F., Witt, C., & Vendeville, B. (2018). Impact of an interbedded viscous décollement on the structural and kinematic coupling in fold-and-thrust belts: Insights from analogue modeling. *Tectonophysics*, *722*, 118–137. <https://doi.org/10.1016/j.tecto.2017.10.019>
- Brocher, T. M., Blakely, R. J., & Wells, R. E. (2004). Reinterpretation of the Seattle uplift, Washington, as a passive roof duplex. *Bulletin of the Seismological Society of America*, *94*(4), 1379–1401. <https://doi.org/10.1785/012003190>
- Buiter, S. J. (2012). A review of brittle compressional wedge models. *Tectonophysics*, *530*, 1–17. <https://doi.org/10.1016/j.tecto.2011.12.018>
- Burkhard, M., & Sommaruga, A. (1998). Evolution of the western Swiss Molasse basin: Structural relations with the Alps and the Jura belt. *Geological Society Special Publication*, *134*(1), 279–298. <https://doi.org/10.1144/GSL.SP.1998.134.01.13>
- Butler, R. W. (1982). The terminology of structures in thrust belts. *Journal of Structural Geology*, *4*(3), 239–245. [https://doi.org/10.1016/0191-8141\(82\)90011-6](https://doi.org/10.1016/0191-8141(82)90011-6)
- Byerlee, J. (1978). Friction of rocks. *PAGEOPH*, *166*, 615–626. <https://doi.org/10.1007/BF00876528>
- Calvín, P., Santolaria, P., Casas, A. M., & Pueyo, E. L. (2018). Detachment fold vs. ramp anticline: A gravity survey in the southern Pyrenean front (External Sierras). *Geological Journal*, *53*(1), 178–190. <https://doi.org/10.1002/gj.2884>
- Choukroune, P., & ECORS team (1989). The ECORS Pyrenean deep seismic profile reflection data and the overall structure of an orogenic belt. *Tectonics*, *8*(1), 23–39. <https://doi.org/10.1029/TC008i001p00023>
- Cobbold, P. R., Clarke, B. J., & Løseth, H. (2009). Structural consequences of fluid overpressure and seepage forces in the outer thrust belt of the Niger Delta. *Petroleum Geoscience*, *15*(1), 3–15. <https://doi.org/10.1144/1354-079309-784>
- Cobbold, P. R., & Rodrigues, N. (2007). Seepage forces, important factors in the formation of horizontal hydraulic fractures and bedding-parallel fibrous veins (“beef” and “cone-in-cone”). *Geofluids*, *7*(3), 313–322. <https://doi.org/10.1111/j.1468-8123.2007.00183.x>
- Costa, E., & Vendeville, B. C. (2002). Experimental insights on the geometry and kinematics of fold-and-thrust belts above a weak, viscous evaporite décollement. *Journal of Structural Geology*, *24*(11), 1729–1739. [https://doi.org/10.1016/S0191-8141\(01\)00169-9](https://doi.org/10.1016/S0191-8141(01)00169-9)
- Couzens-Schultz, B. A., Vendeville, B. C., & Wiltshchko, D. V. (2003). Duplex style and triangle zone formation: Insights from physical modeling. *Journal of Structural Geology*, *25*(10), 1623–1644. [https://doi.org/10.1016/S0191-8141\(03\)00004-X](https://doi.org/10.1016/S0191-8141(03)00004-X)
- Crusafont, M., Riba, O., & Villena, J. (1966). Nota preliminar sobre un nuevo yacimiento de vertebrados aquitanenses en Sta. Cilia (río Formiga; Provincia de Huesca) y sus consecuencias geológicas. In *Notas y Comunicaciones* (Vol. 83, pp. 7–13). Madrid: IGME.
- Cuenca, G., Canudo, J. I., Laplana, C., & Andrés, J. A. (1992). Bio y cronoestratigrafía con mamíferos en la Cuenca Terciaria del Ebro: ensayo de síntesis. *Acta Geológica Hispánica*, *27*(1–2), 127–143.
- Dahlen, F. A. (1990). Critical taper model of fold-and-thrust belts and accretionary wedges. *Annual Review of Earth and Planetary Sciences*, *18*(1), 55–99. <https://doi.org/10.1146/annurev.earth.18.050190.000415>
- Dahlen, F. A., Suppe, J., & Davis, D. (1984). Mechanics of fold-and-thrust belts and accretionary wedges: Cohesive coulomb theory. *Journal of Geophysical Research*, *89*(B12), 10087–10101. <https://doi.org/10.1029/JB089iB12p10087>
- Davis, D., Suppe, J., & Dahlen, F. A. (1983). Mechanics of fold-and-thrust belts and accretionary wedges. *Journal of Geophysical Research*, *88*(B2), 1153–1172. <https://doi.org/10.1029/JB088iB02p01153>
- Davis, D. M., & Engelder, T. (1985). The role of salt in fold and thrust belts. *Tectonophysics*, *119*(1–4), 67–88. [https://doi.org/10.1016/0040-1951\(85\)90033-2](https://doi.org/10.1016/0040-1951(85)90033-2)
- Dean, S. L., Morgan, J. K., & Fournier, T. (2013). Geometries of frontal fold and thrust belts: Insights from discrete element simulations. *Journal of Structural Geology*, *53*, 43–53. <https://doi.org/10.1016/j.jsg.2013.05.008>
- DeCelles, P. G., & Mitra, G. (1995). History of the Sevier orogenic wedge in terms of critical taper models, northeast Utah and southwest Wyoming. *Geological Society of America Bulletin*, *107*(4), 454–462. [https://doi.org/10.1130/0016-7606\(1995\)107%3C0454:HOTSOW%3E2.3.CO;2](https://doi.org/10.1130/0016-7606(1995)107%3C0454:HOTSOW%3E2.3.CO;2)
- Dunn, J. F., Hartshorn, K. G., & Hartshorn, P. W. (1995). Structural styles and hydrocarbon potential of the sub-Andean thrust belt of southern Bolivia. In A. J. Tankard, R. Suárez, & H. J. Welsink (Eds.), *Petroleum Basins of South America* (Vol. 62, pp. 523–543). Tulsa, OK, USA: AAPG Memoir.
- Ezquerro, L. (2017). *El sector norte de la cuenca neógena de Teruel: tectónica, clima y sedimentación*, (Doctoral dissertation) Zaragoza: Universidad de Zaragoza.
- Farran, M. (2008). IMAGE 2SEGY: Una aplicación informática para la conversión de imágenes de perfiles sísmicos a ficheros en formato SEG Y. *Geo-Temas*, *10*, 1215–1218.
- García-Sansegundo, J., García-Senz, J., Montes, M. J., Samsó, J. M., Sanz, J., Teixell, A., & Zamorano, M. (1991). Evolución estructural y sedimentaria del borde norte de la Cuenca del Ebro entre las Sierras Marginales y las Sierras Exteriores. In *I Congreso del Grupo Español del Terciario (Conger’ 91)* (pp. 144–146). Barcelona: Universitat de Barcelona.
- Garrido-Megías, A., & Ríos-Aragüés, L. M. (1972). Síntesis Geológica del Secundario y Terciario entre los ríos Cinca y Segre (Pirineo central de la vertiente sur-pirenaica, provincias de Huesca y Lérida). *Boletín Geológico y Minero de España*, *83*, 1–47.
- GEODE (2011). Mapa Geológico Digital continuo de España [on-line]. In J. Navas (Ed.), *Sistema de Información Geológica Continua: SIGECO*. IGME. [reference date 18/10/2011]. Available in: <http://cuarzo.igme.es/sigeco/default.htm>
- Gil, J. A., & Jurado, M. J. (1994). Evolución tectonoestratigráfica de la terminación occidental del anticlinal de Barbastró–Balaguer. In *II Congreso del Grupo Español del Terciario* (pp. 113–116). Comunicaciones.
- Gil, J. A., & Jurado, M. J. (1998). Geological interpretation and numerical of salt movement in the Barbastró-Balaguer anticline, southern Pyrenees. *Tectonophysics*, *293*(3–4), 141–155. [https://doi.org/10.1016/S0040-1951\(98\)00097-3](https://doi.org/10.1016/S0040-1951(98)00097-3)
- Guillen, A., Calcagno, P., Courriou, G., Joly, A., & Ledru, P. (2008). Geological modelling from field data and geological knowledge, part II —Modelling validation using gravity and magnetic data inversion. *Physics of the Earth and Planetary Interiors*, *171*(1–4), 158–169. <https://doi.org/10.1016/j.pepi.2008.06.014>
- Harrison, J. C. (1995). Tectonics and kinematics of a foreland folded belt influenced by salt, Arctic Canada. In M. P. A. Jackson, D. G. Roberts, & S. Snelson (Eds.), *Salt Tectonics: A Global Perspective* (Vol. 65, pp. 379–412). Tulsa, OK, USA: AAPG Memoir.
- Hilley, G. E., & Strecker, M. R. (2004). Steady state erosion of critical Coulomb wedges with applications to Taiwan and the Himalaya. *Journal of Geophysical Research*, *109*(B1), B01411. <https://doi.org/10.1029/2002JB002284>
- Hogan, P. J., & Burbank, D. W. (1996). Evolution of the Jaca piggy-back basin and emergence of the External Sierras, southern Pyrenees. In P. F. Friend, & C. J. Dabrio (Eds.), *Tertiary Basins of Spain* (pp. 153–160). Cambridge, UK: Cambridge University Press.

- Izquierdo-Llavall, E., Ayala, C., Pueyo, E. L., Casas, A. M., Oliva-Urcia, B., Rubio, F., et al. (2019). Basement-cover relationships and their along-strike changes in the linking zone (Iberian range, Spain): A combined structural and gravimetric study. *Tectonics*, *38*, 2934–2960. <https://doi.org/10.1029/2018TC005422>
- Izquierdo-Llavall, E., Roca, E., Xie, H., Pla, O., Muñoz, J. A., Rowan, M. G., et al. (2018). Influence of overlapping décollements, syntectonic sedimentation, and structural inheritance in the evolution of a contractional system: The Central Kuqa fold-and-thrust belt (Tian Shan Mountains, NW China). *Tectonics*, *37*, 2608–2632. <https://doi.org/10.1029/2017TC004928>
- Jamison, W. R. (1993). Mechanical stability of the triangle zone: The backthrust wedge. *Journal of Geophysical Research*, *98*(B11), 20015–20030. <https://doi.org/10.1029/93JB01233>
- Jardín, A., Chaker, R., & Krzywiec, P. (2007). Understanding seismic propagation through triangle zones, thrust belts and foreland basins. J. Lavé F. Roure & J. Vergés *Thrust Belts and Foreland Basins. From Fold Kinematics to Hydrocarbon Systems* (pp. 63–74). Berlin: Springer.
- Jones, I. F., & Davison, I. (2014). Seismic imaging in and around salt bodies. *Interpretation*, *2*(4), SL1–SL20. <https://doi.org/10.1190/INT-2014-0033.1>
- Jones, P. B. (1996). Triangle zone geometry, terminology and kinematics. *Bulletin of Canadian Petroleum Geology*, *44*, 139–152.
- Keilis-Borok, V. L., & Yanovskaya, T. B. (1967). Inverse problems of seismology. *Geophysical Journal International*, *13*(1–3), 223–234. <https://doi.org/10.1111/j.1365-246X.1967.tb02156.x>
- Konstantinovskaya, E., & Malavieille, J. (2011). Thrust wedges with décollement levels and syntectonic erosion: A view from analog models. *Tectonophysics*, *502*(3–4), 336–350. <https://doi.org/10.1016/j.tecto.2011.01.020>
- Koyi, H. A., & Sans, M. (2006). Deformation transfer in viscous detachments: Comparison of sandbox models to the south Pyrenean triangle zone. *Geological Society of London, Special Publication*, *253*(1), 117–134. <https://doi.org/10.1144/GSL.SP.2006.253.01.06>
- Krzywiec, P., & Vergés, J. (2007). Role of the foredeep evaporites in wedge tectonics and formation of triangle zones: Comparison of the Carpathian and Pyrenean thrust fronts. In O. Lacombe, J. Lavé, F. Roure, & J. Vergés (Eds.), *Thrust belts and foreland basins: From fold kinematics to petroleum systems New Frontiers in Earth Sciences* (pp. 383–394). Verlag: Springer.
- Labauve, P., Meresse, F., Jolivet, M., Teixell, A., & Lahfid, A. (2016). Tectonothermal history of an exhumed thrust-sheet-top basin: An example from the south Pyrenean thrust belt. *Tectonics*, *35*(5), 1280–1313. <https://doi.org/10.1002/2016TC004192>
- Lanaja, J. M. (1987). *Contribución de la exploración petrolífera al conocimiento de la Geología de España* (p. 465). Madrid: IGME 17 maps
- Lebel, D., Langenberg, W., & Mountjoy, E. W. (1996). Structure of the Central Canadian cordilleran thrust-and-fold belt, Athabasca-Brazeau area, Alberta: A large, complex intercutaneous wedge. *Bulletin of Canadian Petroleum Geology*, *44*(2), 282–298.
- Lucha, P., Gutiérrez, F., Galve, J. P., & Guerrero, J. (2012). Geomorphic and stratigraphic evidence of incision-induced halokinetic uplift and dissolution subsidence in transverse drainages crossing the evaporite-cored Barbastro-Balaguer anticline (Ebro Basin, NE Spain). *Geomorphology*, *171–172*, 154–172. <https://doi.org/10.1016/j.geomorph.2012.05.015>
- Luzón, A. (2001). *Análisis Tectosedimentario de los materiales Terciarios continentales del sector central de la Cuenca del Ebro (provincias de Huesca y Zaragoza)*, (Doctoral dissertation) Zaragoza: Universidad de Zaragoza.
- Luzón, A. (2005). Oligocene-Miocene alluvial sedimentation in the northern Ebro Basin, NE Spain. Tectonic control and palaeogeographical evolution. *Sedimentary Geology*, *177*(1–2), 19–39. <https://doi.org/10.1016/j.sedgeo.2005.01.013>
- Martínez-Peña, B. (1991). *La estructura del límite occidental de la unidad surpirenaica central*, (Doctoral dissertation) Zaragoza: Universidad de Zaragoza.
- Martínez-Peña, B., & Pocoví, A. (1988). El amortiguamiento frontal de la estructura de la cobertera Surpirenaica y su relación con el anticlinal de Barbastro-Balaguer. *Acta Geologica Hispánica*, *23*, 81–94.
- Martínez-Peña, M. B., & Casas-Sainz, A. M. (2003). Cretaceous-tertiary tectonic inversion of the Cotiella Basin (southern Pyrenees, Spain). *International Journal of Earth Sciences (Geologische Rundschau)*, *92*(1), 99–113. <https://doi.org/10.1007/s00531-002-0283-x>
- Massoli, D., Koyi, H. A., & Barchi, M. R. (2006). Structural evolution of a fold and thrust belt generated by multiple décollements: Analogue models and natural examples from the northern Apennines (Italy). *Journal of Structural Geology*, *28*(2), 185–199. <https://doi.org/10.1016/j.jsg.2005.11.002>
- McElroy, R. (1990). *Thrust kinematics and syntectonic sedimentation: The Pyrenean frontal ramp, Huesca, Spain*, (Doctoral dissertation) Cambridge: University of Cambridge.
- Millán Garrido, H., Oliva Urcia, B., & Pocoví, J. (2006). The Gavarnie-Guara traverse. Structure and timing of the Gavarnie, Guara-Gèdre and Guarga thrust sheets (Western-Central Pyrenees). *Geogaceta*, *40*, 35–38.
- Millán, H. (1996). *Estructura y cinemática del frente de cabalgamiento Surpirenaico, Sierras Exteriores aragonesas*, (Doctoral dissertation) Zaragoza: Universidad de Zaragoza.
- Millán-Garrido, H., Pueyo-Morer, E. L., Aurell-Cardona, M., Luzón-Aguado, A., Oliva-Urcia, B., Martínez-Peña, M. B., & Pocoví-Juan, A. (2000). Actividad tectónica registrada en los depósitos terciarios del frente meridional del Pirineo central. *Revista de la Sociedad Geológica de España*, *13*(2), 279–300.
- Mochales, T., Casas, A. M., Pueyo, E. L., & Barnolas, A. (2012). Rotational velocity for oblique structures (Boltaña anticline, southern Pyrenees). *Journal of Structural Geology*, *35*, 2–16. <https://doi.org/10.1016/j.jsg.2011.11.009>
- Mochales, T., Pueyo, E. L., Casas, A. M., & Barnolas, A. (2016). Restoring paleomagnetic data in complex superposed folding settings: The Boltaña anticline (southern Pyrenees). *Tectonophysics*, *671*, 281–298. <https://doi.org/10.1016/j.tecto.2016.01.008>
- Mourgues, R., Lacoste, A., & Garibaldi, C. (2014). The Coulomb critical taper theory applied to gravitational instabilities. *Journal of Geophysical Research: Solid Earth*, *119*, 754–765. <https://doi.org/10.1002/2013JB010359>
- Mugnier, J. L., Baby, P., Colletta, B., Vinour, P., Bale, P., & Leturmy, P. (1997). Thrust geometry controlled by erosion and sedimentation: A view from analogue models. *Geology*, *25*(5), 427–430. [https://doi.org/10.1130/0091-7613\(1997\)025%3C0427:TGCBEA%3E2.3.CO;2](https://doi.org/10.1130/0091-7613(1997)025%3C0427:TGCBEA%3E2.3.CO;2)
- Muñoz, A., Arenas, C., González, A., Luzón, A., Pardo, G., & Villena, J. (2002). Ebro basin (northeastern Spain). In W. Gibbons, & T. Moreno (Eds.), *Geology of Spain* (pp. 301–309). (London): Geological Society.
- Muñoz, J. A. (1992). Evolution of a continental collision belt: ECORS-Pyrenees crustal balanced cross-section. In M. Clay (Ed.), *thrust tectonics* (pp. 247–254). London: Chapman & Hall.
- Muñoz, J. A. (2002). Alpine tectonics I: The Alpine system north of the Betic Cordillera. In W. Gibbons, & T. Moreno (Eds.), *Tectonic setting: The Pyrenees Geology of Spain* (pp. 370–385). London: Geological Society.
- Muñoz, J. A., Beamud, E., Fernández, O., Arbués, P., Dinarès-Turell, J., & Poblet, J. (2013). The Ainsa fold and thrust oblique zone of the Central Pyrenees: Kinematics of a curved contractional system from paleomagnetic and structural data. *Tectonics*, *32*, 1142–1175. <https://doi.org/10.1002/tect.20070>
- Muñoz, J. A., Mencos, J., Carrera, N., Gratacós, O., Ferrer, O., & Fernández, O. (2018). The structure of the south-central-Pyrenean fold and thrust belt as constrained by subsurface data. *Geologica Acta*, *16*(4), 439–460. <https://doi.org/10.1344/GeologicaActa2018.16.4.7>

- Navarro, J. J. (1987). Estructura del Somontano de Barbastro. In *Monografía* (p. 100). Huesca: Instituto de Estudios Altoaragoneses.
- Nichols, G. J. (1987). The structure and stratigraphy of the western external sierras of the Pyrenees, northern Spain. *Geological Journal*, 22(3), 245–259. <https://doi.org/10.1002/gj.3350220307>
- Oliva-Urcia, B. (2018). Thirty years (1988–2018) of advances in the knowledge of the structural evolution of the south-Central Pyrenees during the Cenozoic collision, a summary. *Revista de la Sociedad Geológica de España*, 31(2), 51–68.
- Oliva-Urcia, B., Beamud, E., Arenas, C., Pueyo, E. L., Garcés, M., Soto, R., et al. (2019). Dating the northern deposits of the Ebro foreland basin, kinematics of the frontal deformation in the SW Pyrenees. *Tectonophysics*, 765, 11–34. <https://doi.org/10.1016/j.tecto.2019.05.007>
- Oliva-Urcia, B., & Pueyo, E. L. (2007). Gradient of shortening and vertical-axis rotations in the southwestern Pyrenees (Spain). *Revista de la Sociedad Geológica de España*, 20(2), 105–118.
- Ortí, F. (1988). Sedimentación evaporítica continental durante el Terciario de la Península Ibérica: aspectos generales. In *Volumen Simposios II Congreso de Geología de España* (pp. 509–518). Granada.
- Pardo, G., Arenas, C., González, A., Luzón, A., Muñoz, A., Pérez, A., et al. (2004). Cuencas Cenozoicas: La Cuenca del Ebro. In J. A. Vera (Ed.), *Geología de España* (pp. 343–353). Madrid: Sociedad Geológica de España e Instituto Geológico y Minero de España.
- Pardo, G., & Villena, J. (1979). Aportaciones a la geología de la región de Barbastro. *Acta Geológica Hispánica. Homenaje a Solé i Sabaris*, 14, 289–292.
- Pichot, T., & Nalpas, T. (2009). Influence of synkinematic sedimentation in a thrust system with two decollement levels; analogue modelling. *Tectonophysics*, 473(3–4), 466–475. <https://doi.org/10.1016/j.tecto.2009.04.003>
- Pinto, V., Casas, A., Rivero, L., & Torné, M. (2005). 3D gravity modeling of the Triassic salt diapirs of the Cubeta Alavesa (northern Spain). *Tectonophysics*, 405(1–4), 65–75. <https://doi.org/10.1016/j.tecto.2005.05.010>
- Poblet, J., & Lisle, R. J. (2011). Kinematic evolution and structural styles of fold-and-thrust belts. *Geological Society, London, Special Publications*, 349(1), 1–24. <https://doi.org/10.1144/SP349.1>
- Poblet, J., Muñoz, J. A., Anna, T., & Serra-Kiel, J. (1998). Quantifying the kinematics of detachment folds using three-dimensional geometry: Application to the Mediano anticline (Pyrenees, Spain). *Geological Society of America Bulletin*, 110(1), 111–125. [https://doi.org/10.1130/0016-7606\(1998\)110%3C0111:QTKODF%3E2.3.CO;2](https://doi.org/10.1130/0016-7606(1998)110%3C0111:QTKODF%3E2.3.CO;2)
- Pocoví, A. (1978). Estudio geológico de las Sierras Marginales Catalanas (Prepirineo de Lerida). *Acta Geologica Hispánica*, 13, 73–80.
- Pocoví, A. (1979). Deformaciones de la cobertera despegada influidas por accidentes de zócalo en las Sierras Marginales Catalanas (Pirineo Meridional). *Acta Geologica Hispánica*, 14, 143–148.
- Press, F. (1968). Earth models obtained by Monte Carlo inversion. *Journal of Geophysical Research*, 73(16), 5223–5234. <https://doi.org/10.1029/JB073i016p05223>
- Press, F. (1970). Earth models consistent with geophysical data. *Physics of the Earth and Planetary Interiors*, 3, 3–22. [https://doi.org/10.1016/0031-9201\(70\)90039-7](https://doi.org/10.1016/0031-9201(70)90039-7)
- Price, R. A. (1981). The cordilleran foreland thrust and fold belt in the southern Canadian Rocky Mountains. In K. R. McClay, & N. Price (Eds.), *Thrust and Nappe tectonics* (Vol. 9, pp. 427–448). London: Geological Society of London, Special Publications.
- Pueyo, E. L., Izquierdo-Llavall, E., Rodríguez-Pintó, A., Rey, M. C., Oliva-Urcia, B., Casas, A. M., et al. (2016). Petrophysical properties in the Iberian range and surrounding areas (NE Spain): 1-Density. *Journal of Maps*, 12(5), 836–844. <https://doi.org/10.1080/17445647.2015.1084545>
- Pueyo, E. L., Millán, H., & Pocoví, A. (1997). Rotational kinematics of the southpyrenean basal thrust at the Sierras Exteriores Aragonesas: Magnetotectonic data. *Acta Geologica Hispánica*, 32(3–4), 119–138.
- Pueyo, E. L., Millán, H., & Pocoví, A. (2002). Rotation velocity of a thrust: A paleomagnetic study in the external sierras (southern Pyrenees). *Sedimentary Geology*, 146(1–2), 191–208. [https://doi.org/10.1016/S0037-0738\(01\)00172-5](https://doi.org/10.1016/S0037-0738(01)00172-5)
- Puigdefàbregas, C. (1975). La sedimentación molásica en la cuenca de Jaca. *Pirineos*, 104, 1–188.
- Puigdefàbregas, C., Muñoz, J. A., & Vergés, J. (1992). Thrusting and foreland basin evolution in the southern Pyrenees. In *Thrust tectonics* (pp. 247–254). Dordrecht: Springer.
- Quirantes, J. (1969). *Estudio sedimentológico y estratigráfico del Terciario continental de Los Monegros.* (Doctoral dissertation) Granada: Universidad de Granada.
- Riba, O., & Llamas, M. R. (1962). Los terrenos yesíferos triásicos y terciarios de las proximidades de Estada (Huesca). In *I Coloquio Internacional sobre las obras públicas en los terrenos yesíferos* (pp. 107–120). Madrid-Zaragoza-Sevilla: Servicio Geológico de Obras Públicas, Tema 6°.
- Riba, O., Reguant, S., & Villena, J. (1983). Ensayo de síntesis estratigráfica y evolutiva de la cuenca terciaria del Ebro. In J. M. Ríos (Ed.), *Geología de España, II, Libro Jubilar J.M. Ríos* (131–159). Madrid: IGME.
- Ríos, J. M. (1948). *Diapirismo* (p. 50). Madrid: Boletín del Instituto Geológico y Minero de España.
- Rodríguez-Pintó, A. (2012). *Magnetoestratigrafía del Eoceno inferior y medio en el frente Surpirenaico (Sierras Exteriores): Implicaciones cronoestratigráficas y cinemáticas.* (Doctoral dissertation) Zaragoza: Universidad de Zaragoza.
- Rodríguez-Pintó, A., Pueyo, E. L., Calvin, P., Sánchez, E., Ramajo, J., Ramón, M. J., et al. (2016). Rotational kinematics of a curved fold: A structural and paleomagnetic study in the Balzes anticline (southern Pyrenees). *Tectonophysics*, 677–678, 171–189. <https://doi.org/10.1016/j.tecto.2016.02.049>
- Roest, W. R., & Srivastava, S. P. (1991). Kinematics of the plate boundaries between Eurasia, Iberia, and Africa in the North Atlantic from the Late Cretaceous to the present. *Geology*, 19(6), 613–616. [https://doi.org/10.1130/0091-7613\(1991\)019%3C0613:KOTPB%3E2.3.CO;2](https://doi.org/10.1130/0091-7613(1991)019%3C0613:KOTPB%3E2.3.CO;2)
- Rosenbaum, G., Lister, G. S., & Duboz, C. (2002). Relative motions of Africa, Iberia and Europe during Alpine orogeny. *Tectonophysics*, 359(1–2), 117–129. [https://doi.org/10.1016/S0040-1951\(02\)00442-0](https://doi.org/10.1016/S0040-1951(02)00442-0)
- Roure, F., Choukroune, P., Berastegui, X., Mufioz, J. A., Villien, A., Matheron, P., et al. (1989). ECORS deep seismic data and balanced cross-sections: Geometric constraints on the evolution of the Pyrenees. *Tectonics*, 8(1), 41–50. <https://doi.org/10.1029/TC008i001p00041>
- Sans, M. (2003). From thrust tectonics to diapirism. The role of evaporites in the kinematic evolution of the eastern south Pyrenean front. *Geologica Acta*, 1(3), 239–259. <https://doi.org/10.1344/105.000001613>
- Sans, M., Muñoz, J. A., & Vergés, J. (1996). Triangle zone and thrust wedge geometries related to evaporitic horizons (southern Pyrenees). *Bulletin of Canadian Petroleum Geology*, 44(2), 375–384.
- Santolaria, P., Casas, A., Casas-Sainz, A. M., & Soto, R. (2016). Gravimetric modelling to assess salt tectonics in the western end of the south Pyrenean central unit. *Journal of the Geological Society*, 174(2), 269–288. <https://doi.org/10.1144/jgs2016-027>
- Santolaria, P., Luzón, A., Casas, A., & Soto, R. (2015). Coupling far and near tectonic signals in syn-orogenic sediments: The Olvena growth strata (Sierras Marginales, southern Pyrenees). *Geologica Acta*, 13(4), 297–308. <https://doi.org/10.1344/GeologicaActa2015.13.4.3>

- Santolaria, P., Vendeville, B. C., Graveleau, F., Soto, R., & Casas-Sainz, A. M. (2015). Double evaporitic décollements: Influence of pinch-out overlapping in experimental thrust wedges. *Journal of Structural Geology*, *76*, 35–51. <https://doi.org/10.1016/j.jsg.2015.04.002>
- Selzer, G. (1934). Geologie der südpirenaischen Sierrren in Oberaragonien. In *Neves Jahrbuch für Min. Geol. und Pal.*, *71*, Beilage Band, *Stuttgart* (Vol. 4, pp. 370–406). Madrid, Spain.
- Senz, J. G., & Zamorano, M. (1992). Evolución tectónica y sedimentaria durante el Priaboniense superior-Mioceno inferior, en el frente de cabalgamiento de las Sierras Marginales Occidentales. *Acta Geologica Hispánica*, *27*(1–2), 195–209.
- Sherkati, S., Letouzey, J., & Frizon de Lamotte, D. (2006). Central Zagros fold-thrust belt (Iran): New insights from seismic data, field observation, and sandbox modelling. *Tectonics*, *25*, TC4007. <https://doi.org/10.1029/2004TC001766>
- Smit, J. H. W., Brun, J. P., & Soukoutis, D. (2003). Deformation of brittle–ductile thrust wedges in experiments and nature. *Journal of Geophysical Research*, *108*(B10), 2480. <https://doi.org/10.1029/2002JB002190>
- Suppe, J. (2007). Absolute fault and crustal strength from wedge tapers. *Geology*, *35*(12), 1127–1130. <https://doi.org/10.1130/G24053A.1>
- Tarantola, A. (2005). *Inverse problem theory and Methods for Model Parameter Estimation* (p. 342). Philadelphia, PA: SIAM.
- Teixell, A. (1998). Crustal structure and orogenic material budget in the west central Pyrenees. *Tectonics*, *17*(3), 395–406. <https://doi.org/10.1029/98TC00561>
- Turienzo, M., Sánchez, N., Lebinson, F., Peralta, F., Araujo, V., Irastorza, A., & Dimieri, L. (2020). Basement-cover interaction in the mountain front of the northern Neuquén fold and thrust belt (37°10'–37°40'S) Argentina. *Journal of South American Earth Sciences*, *100*. <https://doi.org/10.1016/j.jsames.2020.102560>
- Vergés, J., & Burbank, D. W. (1996). Eocene-Oligocene thrusting and basin configuration in the eastern and central Pyrenees (Spain). *Tertiary basins of Spain: the stratigraphic record of crustal kinematics*, *6*, 120. <https://doi.org/10.1017/cbo9780511524851.020>
- Vergés, J., & García-Senz, J. M. (2001). Mesozoic evolution and Cenozoic inversion of the Pyrenean rift. In P. A. Ziegler, W. Cavazza, A. H. F. Robertson, & S. Crasquin-Soleau (Eds.), *Peri-Tethyan rift/wrench basins and passive margins* (Vol. 186, pp. 187–212). Paris: Mémoires Muséum National d'Histoire Naturelle.
- Vergés, J., Muñoz, J. A., & Martínez, A. (1992). South Pyrenean fold and thrust belt: The role of foreland evaporitic levels in thrust geometry. In *Thrust tectonics* (pp. 255–264). Dordrecht: Springer.
- von Hagke, C., Cederbom, C. E., Oncken, O., Stöckli, D. F., Rahn, M. K., & Schlunegger, F. (2012). Linking the northern Alps with their foreland: The latest exhumation history resolved by low-temperature thermochronology. *Tectonics*, *31*, 1–25. <https://doi.org/10.1029/2011tc003078>
- von Hagke, C., & Malz, A. (2018). Triangle zones—Geometry, kinematics, mechanics, and the need for appreciation of uncertainties. *Earth-Science Reviews*, *177*, 24–42. <https://doi.org/10.1016/j.earscirev.2017.11.003>